INVESTIGATION INTO PRYING FORCE AND BOLT MOMENT IN WELDED STEEL T-STUBS

Tchabremane Jean de la Croix KOMBATE[1], Kıvanç TAŞKIN[2*], Kerem PEKER[3]

[1] Department of Civil Engineering, Eskişehir Technical University, Eskişehir, Türkiye
ORCID No: https://orcid.org/0000-0002-5366-0315
[2] Department of Civil Engineering, Eskişehir Technical University, Eskişehir, Türkiye
ORCID No: https://orcid.org/0000-0001-8024-4600
[3] Erdemli Engineering and Consulting Ltd., İstanbul, Türkiye
ORCID No: https://orcid.org/0000-0003-0760-6964

Keywords

Steel connections
Bolted connection
T-stub
Prying effect
Bolt bending

Abstract

Prying action may develop in bolted T-stub connection due to the flange deformation. In this paper, an extensive numerical study was carried out on welded plate T-stubs to investigate prying action. Using experimental data in the literature, a finite element model was constructed and validated in ABAQUS. Good agreement was obtained, and over 200 FE models were generated to study the influence of flange thickness, edge distance, and gauge distance on the behavior of bolted T-stubs, including prying effects. The resistance predictions provided in EN 1993-1-8 were found to be conservative. This study's novelty was the focus on the bending moment that may develop in the bolts. Tests have highlighted the flexural engagement of the bolts. Combined with tensile action in the bolts, it may induce substantial stresses and cause premature failure. Few studies have been dedicated to investigating the bending moment in the bolts. Consequently, the actual codes do not account for the bending moment in the bolts. It was found that the bolt moment could be considerable and should be accounted for in the design procedure. The influence of several geometrical properties on the bolt moment was investigated. Additionally, the M-N interaction curves examined the combined action of tension and bending in the bolts.

BULONLU ÇELİK BİRLEŞİMLERDEKİ KANIRTMA ETKİSİNİN ARAŞTIRILMASI

Anahtar Kelimeler

Çelik birleşimler
Civatalı bağlantılar
T-parça
Kanırtma etkisi
Cıvata bükülme

Öz

Çelik yapılarda taşıyıcı elemanların en yaygın birleşim şekli olan T birleşim bölgelerinde ortaya çıkan davranışın ortak özelliği çekme yükünden dolayı başlık bölgelerinde oluşan deformasyonlardır. Buna sebep olan etki de kanırtma (prying) etkisidir. Bulonlardaki eğilme momentinin incelenmesine yönelik çok az çalışma yapılmıştır. Literatürde verilen testler bulonların eğilme etkisini vurgulamaktadır. Bu çalışmada, kanırtma etkilerini araştırmak için kaynaklı plakalar ile oluşturulan T-birleşimler üzerinde kapsamlı bir parametrik çalışma gerçekleştirilmiştir. ABAQUS'ta oluşturulan gelişmiş sonlu eleman modellerini kalibre etmek ve doğrulamak için literatürdeki deneysel veriler kullanılmıştır. Flanş kalınlığı, kenar mesafesi ve bulonların arasındaki mesafe gibi parametrelerin bulonlu T-birleşimlerin davranışı ve özellikle kanırtma etkisi üzerindeki etkilerini incelemek için 200'den fazla sonlu eleman modeli oluşturulmuştur. EN 1993-1-8'de verilen dayanım tahminlerinin çok güvenli olduğu görülmüştür. Bu çalışmadaki bir yenilik de bulonlarda oluşabilecek eğilme momentine odaklanılmasıdır. Bulonlardaki çekme kuvvetleri ile birleştiğinde, önemli gerilmelere neden olmakta ve taşıma kapasitesine gelmeden erken göçmeye yol açabilmektedir. Sonuç olarak, mevcut standartlar bulonlardaki eğilme momentini hesaba katmamaktadır. Bulonda oluşacak momentin önemli olabileceği ve tasarım aşamasında hesaba katılması gerektiği görülmektedir. Farklı geometrik özelliklerin bulon momenti üzerindeki etkisi araştırılmıştır. Ayrıca, bulonlardaki gerilme ve eğilmenin birleşik etkisi M-N etkileşim eğrileri aracılığıyla incelenmiştir.

Araştırma Makalesi		Research Article	
Başvuru Tarihi	: 22.04.2024	Submission Date	: 22.04.2024
Kabul Tarihi	: 19.12.2024	Accepted Date	: 19.12.2024

* Sorumlu yazar: kivanct@eskisehir.edu.tr
https://doi.org/10.31796/ogummf.1471916

1. Introduction

Connections play a crucial role in the safety and stability of structures. Due to their easy fabrication, installation, and ductile behavior, bolted connections are now preferred to welded connections in steel structures. However, steel bolted connections involve various components and nonlinearities (such as material nonlinearities and contact nonlinearities), resulting in a nonlinear behavior that is complex to determine. Approximations are often necessary to incorporate the actual behavior into everyday design because of its complexity. One of these approximations is the equivalent T-stub model, which has been widely investigated before its implementation in EN 1993-1-8.

Finite element modeling can be used as an alternative to experimentation. In fact, besides being less demanding, FE models can yield results that are in agreement with experiments. Also, they can describe phenomena such as contact stress distribution that cannot be accurately measured experimentally. Finally, various configurations can be covered, allowing for parametrical studies and analytical formulations. The last decades have seen increasing use of FE modeling due to progress in computer technology and non-linear numerical algorithms. The contributions of Sherbourne and Bahaari (1996); Mistakidis, Baniotopoulos, Bisbos, and Panagiotopoulos (1997); Bursi and Jaspart (1997, 1997, 1998); Wanzek and Gebbeken (1999); Swanson, Kokan, and Leon (2002); and Lemonis and Gantes (2003) helped put in place guidelines for the construction of efficient finite element models that could realistically reproduce the behaviour of bolted T-stub connections.

One common and significant behavioral characteristic of nearly all types of tensile bolted connections is prying action. Tests have shown that the flexural deformation of the flanges of the connected members can subject bolts to additional forces and moments. Prying action can significantly increase the bolt load and cause bolts to fail before the applied tension has reached the design tension load. Therefore, not taking into consideration prying action could lead to unsafe design. Although several researchers reported the bending of bolts at failure and its influence on the performance of T-stubs, the prying effect is commonly taken into account by only increasing the axial force in the bolt.

The earliest studies on T-stubs and prying action include that of Nair, Birkemoe, and Munse (1969) who carried out an experimental and analytical study to determine the behavior of ASTM A325 and A490 high strength bolts loaded in direct tension in tee-connections, and formulate methods for the design of such connections. Douty and McGuire (1974) performed experiments on various T-stubs and developed a semi-empirical equation for evaluating the prying force Q at the ultimate load. Zoetemeijer (1974) studied the tension side of bolted beam-to-column connections and emphasized the role of prying force in the failure mode of the T-stub. He expressed the maximum prying force Qmax as a function of the moment of the flange and the edge distance. Agerskov (1977) conducted a series of tests to measure prying force for different geometries. In some significant respects, the author presented a formulation similar to that of Douty and McGuire (1974), with the difference being that the effect of shear stresses was considered. The actual formulations presented in AISC are the fruition of the work of Thornton (1985); Swanson and Leon (2000); Kulak, Fisher and Struik (2001); and Swanson, Kokan, and Leon (2002).

Several other others conducted studies about prying forces. Chasten, Lu, and Driscoll (1992) investigated the contact force distribution. Following an analytical study aiming to determine the magnitude and location of the prying forces, the authors found that the prying force resultant is not located at the plate edge and recommended using a conservative $x = 0.6l_v$for design purposes.

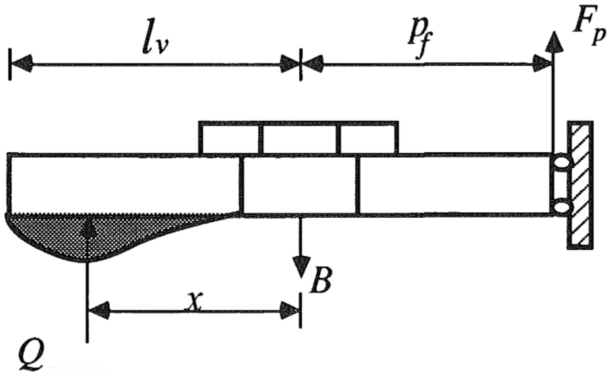

Fig. 1. Contact pressure bulb

Using the results of 1800 FE analyses of L and T bolted connections, Atasoy (2012) suggested some corrections for the expressions formulated by Douty and McGuire and Struik and de Back, depending on the ratio of the flange thickness to the bolt diameter. Rassati, 2012; Hantouche and Abboud, 2014; Hantouche, Kukreti, and Rassati, 2015; Hantouche, Kukreti, Rassati, and Swanson, 2015) were used to develop two prying models that predict the failure strength of thick-flange built-up T-stub connections with complete joint penetration (CJP) and fillet welds.

Through an experimental and numerical program, Yang, Kim, Park, and Back (2013) and Yang, Park, Kim, and Back (2013) suggested an analytical model which takes into account prying action for the prediction of the initial axial stiffness and the ultimate strength. The authors also suggested correcting the bolt action line based on bolt stress distribution obtained from the numerical analysis. A mechanical proposed a mechanical model, based on an improved beam model and validated using 3D finite element models, was proposed by model Couchaux, Hjiaj, Ryan, and Bureau (2017) allowing for the assessment of the total bolt force, separation length, and prying force location. The authors concluded that the magnitude of the external load did not affect the contact zone length in a non-preloaded connection. Bezerra, Bonillab, Silvac, and Matias (2020) conducted a numerical investigation into the influence of the flange thickness on the magnitude and location of the prying force. The authors concluded that the existing analytical models, which assumes a fixed location of the prying force, could not adequately represent the prying action (Kombate and Taşkın, 2022).

In most studies, the prying effect is taken into account by only considering the supplementary axial force in the bolt, although several researchers reported the bending of bolts at failure (Kulak et al., 2001; Piluso, Faella, and Rizzano, 2001; Swanson et al., 2002; Girão Coelho, 2004; Girão Coelho, Bijlaard, and Gresnigt; 2004; Baoa et al., 2019; Yuan et al., 2020). Authors such as Piluso and Rizzano (2008) and Hu, Leon, and Park (2011, 2012) recommended that bolt bending should be considered in the design model.

The deformation of the connected parts can result in the bending of the bolt even when there is no significant increase in bolt axial force (Kulak et al., 2001). Few studies have been dedicated to evaluating the bending moment in bolts. Using 3D finite element analysis of T-stubs, Abidelah, Bouchaïr, and Kerdal (2014) studied the influence of bolt bending. Furthermore, the authors suggested considering the effect of the bolt bending by adding rotational springs. Herrera, Desjouis, Gomez, and Sarrazin (2008) performed a series of tests on one-half-scale built-up T-stubs specimens. Detailed 3D finite element models of the tested specimens were generated and could adequately capture the bending of the tension bolts produced by the prying of the T flange. Stamatopoulos and Ermopoulos (2010) proposed a design procedure for T-stubs, considering bolt bending. The influence of the developed bending on the strength of bolts was determined by evaluating the interaction between the bending moment and the axial tensile force (Abidelah et al., 2014; Stamatopoulos and Ermopoulos, 2010). More studies devoted to flexural engagement are necessary to provide more insight into the behavior of bolted T-stubs, allowing for improved formulations and adequate design of bolted connections.

A parametric study incorporating 226 models has been carried out to examine the influence of the flange thickness, the edge distance, and the gauge distance on prying effects in bolted T-stubs. Various elements related to prying action were investigated, including total bolt force, the prying force, and the magnitude and location of the resultant contact forces. Furthermore, the moment the bolts may be subjected to was considered, and its variation in function of the flange thickness, the edge distance, and the gauge distance was examined.

2. Finite Element Modelling

A finite element model is developed in ABAQUS and calibrated with data obtained from the experiments conducted by Girão Coelho (2004) and Bursi and Jaspart (1997).

The specimens WT1g and T1 are selected for the calibration procedure. The geometrical characteristics of the specimens are depicted in Fig. 2 and specified in Table 1.

Table 1. Geometrical Properties of the Specimens

	Specimen WT1g	Specimen T1
n	30 mm	30 mm
w	90 mm	90 mm
e_1	20 mm	20 mm
p	50 mm	40 mm
t	10 mm	10.7 mm
t_w	10 mm	7.1 mm
a_w	5 mm	-
$\emptyset_b$	12 mm	12 mm

n: edge distance; t: flange thickness
w: gauge distance; t_w: web thickness
e_1: end distance; a_w: weld throat thickness
p: pitch of the bolts; $\emptyset_b$: bolt diameter

2.1. Model Description

It is possible to avoid modeling the whole T-stub using symmetry, if any. Generally, YZ and YX planes may be geometrical planes of symmetry. However, the XZ plane cannot be strictly considered a symmetry plane because the bolt heads and nuts generally possess different rigidities. For this reason, only YZ and YX symmetry planes were considered, allowing for a reduction, as illustrated in Fig. 3. The hot-rolled T-stub was modeled in one block, including the web, flange, and fillet radius. In contrast, the different elements were modeled separately and assembled using adequate boundary and contact interactions for the welded plate T-stub. The components-webs, flanges, welds, and bolts – were meshed using solid elements C3D8R (i.e., 8-node linear brick with reduced integration). C3D8R elements, which present advantages such as reduced computation time and hourglass control, yielded satisfactory results. The bolt hole and shank were taken equal to the nominal bolt diameter. Considering that the bolt head and nut dimensions were not provided, the nominal values mentioned in DIN EN 14399-4 were used (See Table 2). Also, the washers were not modeled in compliance with the experimental conditions.

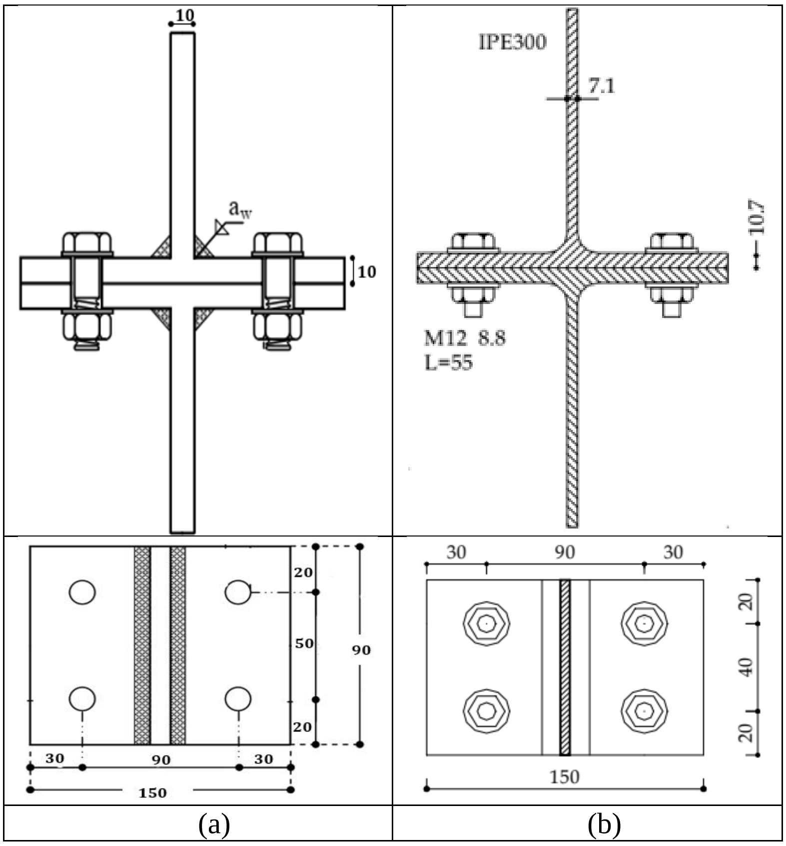

Fig. 2. Geometrical Characteristics and Cross-section of (a) WT1g Specimen and (b) T1 Specimen

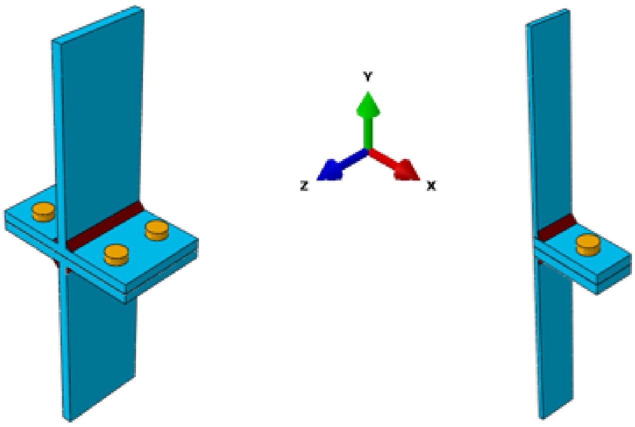

Fig. 3. Original WT1g model and its reduced model

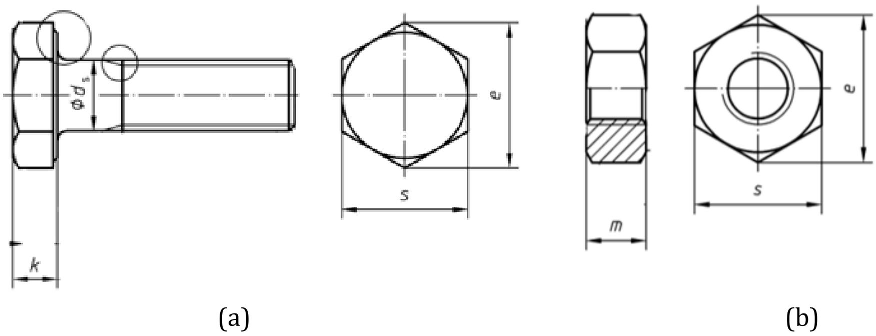

Fig. 4. Bolt head and nut Dimensions

Table 2. Bolt Head and Nut Dimensions for M12 bolts

Bolt Head		Nut	
k	s	m	s
8 mm	22 mm	10 mm	22 mm

The FE models included all nonlinearities, such as contact nonlinearities and material behavior. An elastoplastic constitutive law with isotropic strain hardening based on the Von Mises yield criterion was adopted for material nonlinearity. The failure condition was set as the attainment of the ultimate strain (ε_u), either for the bolt or any component of the T-section.

2.2. Material Properties

An elastoplastic constitutive law with isotropic strain hardening based on the Von Mises yield criterion is adopted for material nonlinearity. The failure condition was set as the attainment of the ultimate strain other than the bolt or any component of the T-section. For good correlation with experimental results, the entire stress-strain curves of the materials were adopted in the FE models (see Fig. 5). As a simplification, the welds in the WP-T-stubs were provided the same material properties as the T-flanges and T-webs. For the parametrical study, the same material properties were used for all the thicknesses based on the similarities of the actual stress-strain curves for flange thicknesses of 10, 15, and 20 mm (Faralli, Latour, Tan, Rizzano, and Wrobel; 2021). To extend the study of the behavior of T-stubs with thin flanges, 8 mm thickness was also included.

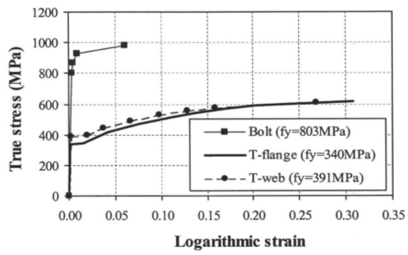

(a)

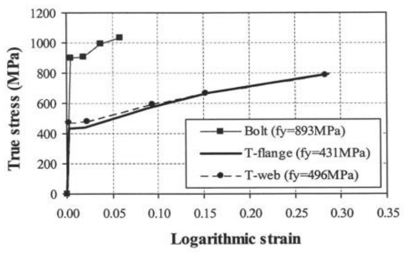

(b)

Fig. 5. Strain-Stress Material Laws: (a) Specimen WT1g (Girão Coelho, 2004) and (b) Specimen T1 (Bursi and Jaspart, 1997)

2.3. Boundary Conditions and Loading

Adequate boundary conditions and loading patterns are among the requirements for an efficient numerical simulation. The boundary conditions should reflect those of the tests. Hence, the end of the lower T-web was fully fixed; only the end of the upper T-web was allowed to move in the direction of the applied load. In the model intended for validation, a reduced model could be obtained using both X- and Z-symmetry boundary conditions (See Fig. 6). As for the models included in the parametrical study, only X-symmetry was considered. In fact, unlike the initial T-stubs that had four bolts and a width $2b = 2e_1 + p$ (see Fig. 2), the T-stubs involved in the parametrical study had only two bolts and a width $b = 2e_1$ (see Fig. 7).

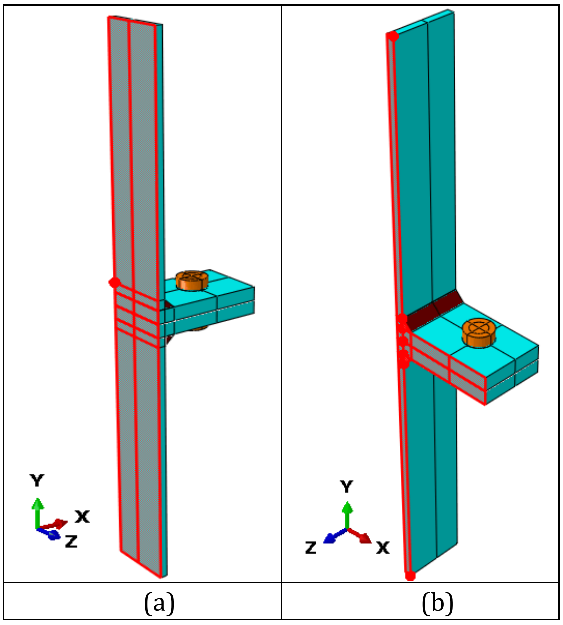

Fig. 6. Symmetry Applied in (a) X-Direction And (b) in Z-Direction

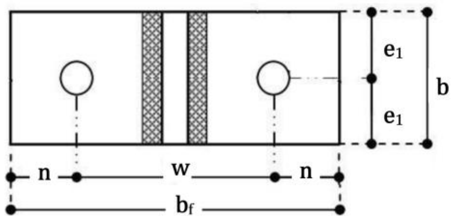

Fig. 7. Geometrical Characteristics of the Specimens Involved in the Parametrical Study

Regarding contact interactions, standard surface-to-surface formulation with finite sliding was defined. The considered pairs were:

- Bolt head and nut – flanges
- Flanges – webs
- Upper flange – Lower flange
- Bolt shank – Bolt hole

The contact properties were defined such that the expected behavior was simulated with hard contact, while the classic isotropic Coulomb friction law was used to model the tangential behavior. A penalty friction coefficient of 0.25 was taken, as suggested by Coelho et al. (2004). In reality, the bolt holes are more significant than the bolt diameters, so frictionless contact properties were considered in the hole area. Additionally, tie constraints attached the welds to the T-web and the T-flange.

The load was applied at the top of the upper T-web in the positive Y-direction using displacement control (See Fig. 8). Although both displacement-controlled and load-controlled analyses were compared and yielded similar results, displacement control was selected because it could offer better convergence conditions [30].

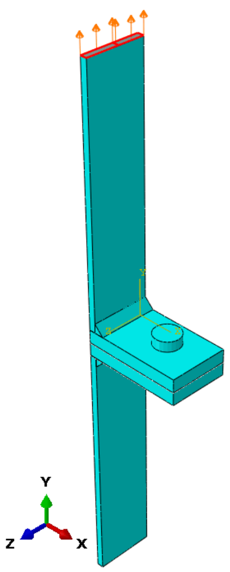

Fig. 8. Load Application

2.4. Model validation

A mesh sensitivity study was carried out to obtain a model with satisfactory results and acceptable computation time, and the mesh size and the flange discretization (number of elements through the thickness) were investigated. The bolt and the T-stub mesh sizes were identical and chosen proportionally to the thickness of the T-stub flange. Three mesh sizes were examined: $t_f/3$, $t_f/5$ and $t_f/10$. An element size of $t_f/3$ was deemed adequate. In the aftermath, T-stub models with different flange discretizations were investigated. Previous studies concluded that for bending problems, a minimum of three elements through the plate thickness is recommended to ensure accurate results (Bursi and Jaspart, 1997). Consequently, models with 3, 4, 5, 7, and 10 elements through the flange thickness were compared. The model with seven elements through the flange was chosen because it yielded satisfactory results within a reasonable computation time.

For the model validation, it is essential to compare the load-deformation curve, which is the most significant characteristic describing the overall behavior of the model, as well as the failure mode. The force-displacement curve obtained from the FE analysis showed satisfactory agreement with the experimental force-displacement curve (Fig. 8). For the T-stub specimen WT1g, the experimental observations indicated that, at a deformation level around 14 mm, there was a smooth drop of load that continued until bolt fracture at 20.5 mm. Consequently, the curve obtained from the finite element modeling stopped at a deformation level of 13.5 mm, showing a good agreement with the experimental results. As for the T-stub specimen T1, an ultimate deformation of 9.20 mm was reached, which is very close to the experimental value of 9.49 mm. For both specimens, the experimental observations revealed combined failure involving significant flange yielding (with cracking of the flange in the heat-affected zone of the welds for WT1g) and bolt fracture. Although the experimental cracking in the welded zone was not observed in the finite element model, a pronounced yielding was observed. The difference may derive from the modeling the fillet weld and the heat-affected zone near the weld toe. The welding process can render the material more brittle. These effects are complex to quantify and take into consideration. Therefore, they were not included in the simulations, and the welds in the WP-T-stubs were provided with the same material properties as the T-flanges and T-webs.

3. Parametric Investigation

Following the validation of the numerical model, 226 models were generated to study the influence of parameters such as flange thickness, t , edge distance, n, and gauge distance, w. The edge distance and gauge distance value ranges were chosen in agreement with the provisions of EN 1993-1-8 (Table 3). The geometrical characteristics of the specimens are depicted in Fig. 7 and specified in Table 4.

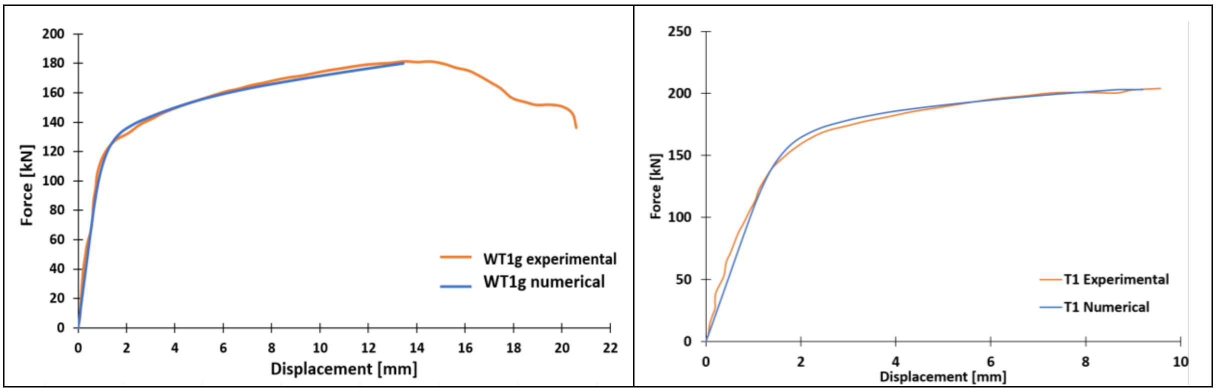

Fig. 9. Experimental and Numerical F-D Curves of (a) WT1g and (b) T1 Specimens

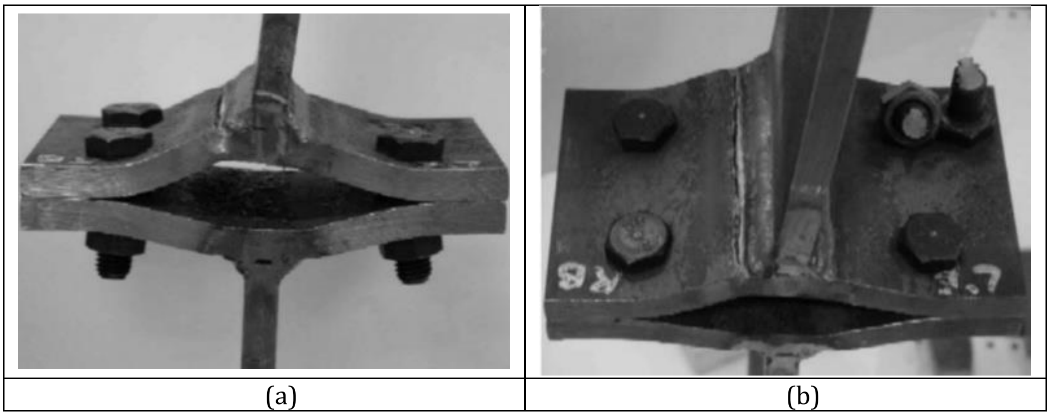

Fig. 10. Front View and Top View of Specimens WT1g After Failure

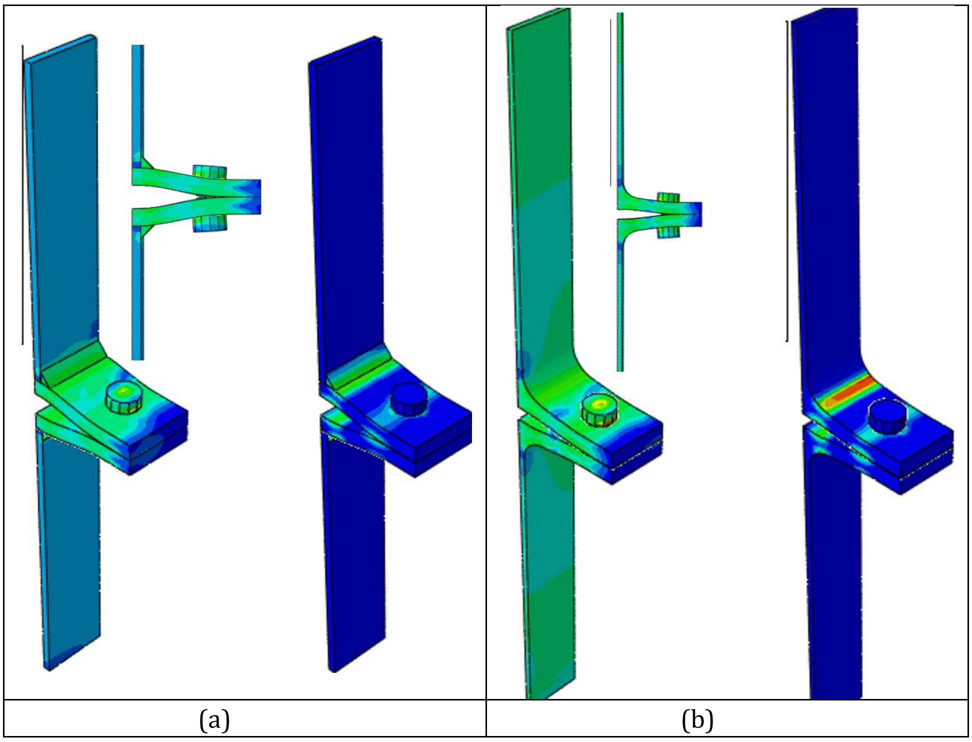

Fig. 11. Deformation and Yielding Status at the Ultimate Stage of (a) Specimen WT1g and (b) Specimen T1

Table 3. Minimum and Maximum Edge Distance and Gauge Distance Allowed by EN 1993-1-8

Parameter	Minimum value according to EN 1993-1-8	Maximum value according to EN 1993-1-8
Edge Distances	14.4 mm	50 mm for t = 8 mm 80 mm for t = 10 mm 100 mm for t = 15 mm 120 mm for t = 20 mm
Gauge Distances (spacing)	26.4 mm	110 mm for t = 8 mm 140 mm for t = 10 mm 200 mm for t = 15 mm 200 mm for t = 20 mm

Table 4. Geometrical Properties of the Specimens of the Parametrical Study

	Parametrical study			
	$t = 8\ mm$	$t = 10\ mm$	$t = 15\ mm$	$t = 20\ mm$
n	15 – 50 [mm]	15 – 70 [mm]	15 – 100 [mm]	15 – 100 [mm]
w	50 – 110 [mm]	50 – 140 [mm]	60 – 200 [mm]	70 – 200 [mm]
e_1	50 mm	50 mm	50 mm	50 mm
$t = t_w$*	8 mm	10 mm	15 mm	20 mm
a_w	5 mm	5 mm	8 mm	8 mm
$\emptyset_b$*	12 mm	12 mm	12 mm	12 mm

* t: flange thickness t_w: web thickness $\emptyset_b$: bolt diameter

The same material properties were used for all the thicknesses based on the similarities of the accurate stress-strain curves for flange thicknesses of 10, 15, and 20 mm (Faralli et al., 2021). To extend the study of the behavior of T-stubs with thin flanges, 8 mm thickness was also included. Considering the different flange thicknesses, the number of elements through the flange was also examined for each thickness, while keeping the initial mesh size.

3.1. Failure Modes

Regarding steel T-stubs, the EN 1993-1-8 highlights three possible failure modes: complete yielding of the flange (Mode 1), bolt failure with yielding of the flange (Mode 2), and bolt failure (Mode 3). Failure mode 2 was observed in specimens with 8 mm and 10 mm flange thickness. Minor flange deformation occurred for short gauge distances, and the bolt was subjected to minor flexural deformation. As the gauge distance increased, the failure mechanism shifted closer to mode 1. The flange exhibited double curvature deformation, and the bending of the bolt was more pronounced (Fig. 12, Fig. 13).

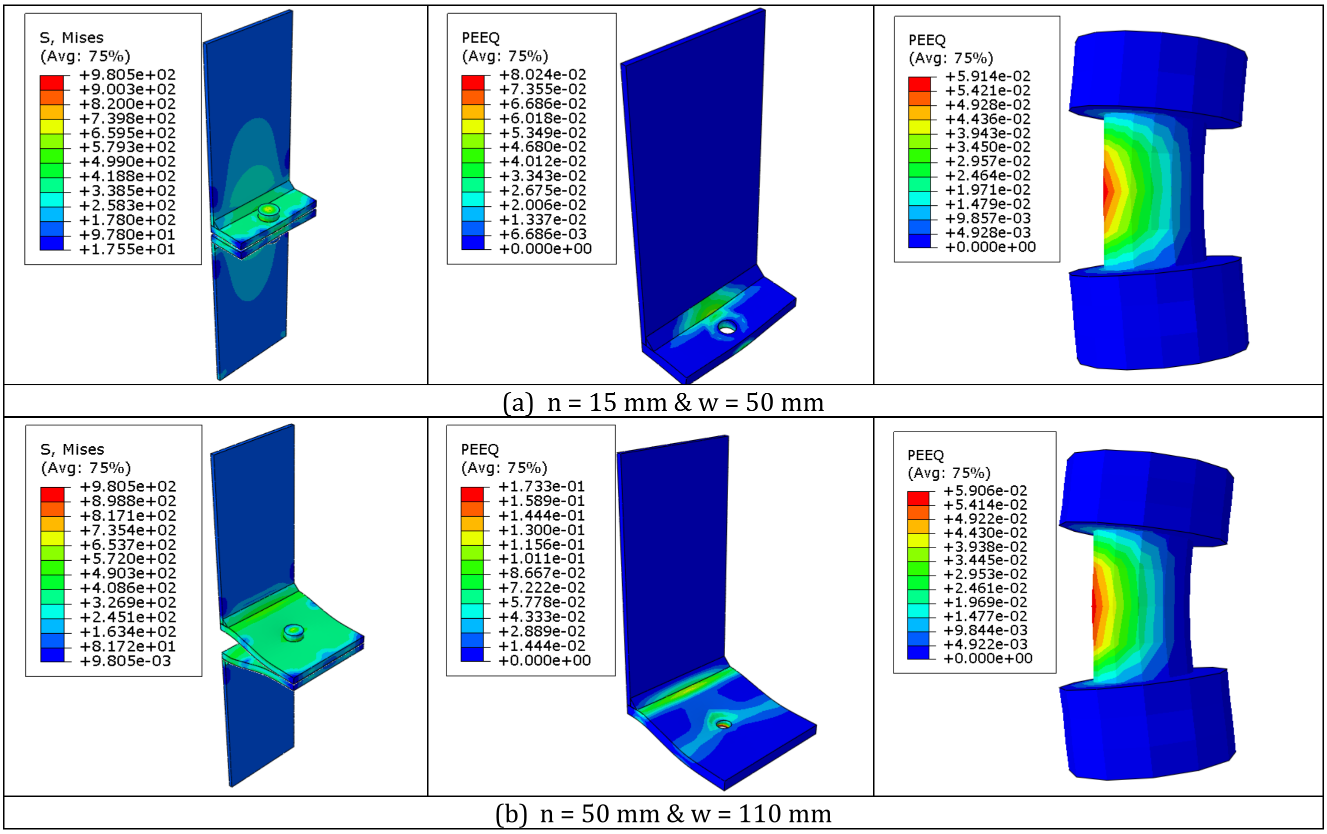

Fig. 12. Ultimate Stage of Specimens of t = 8 mm

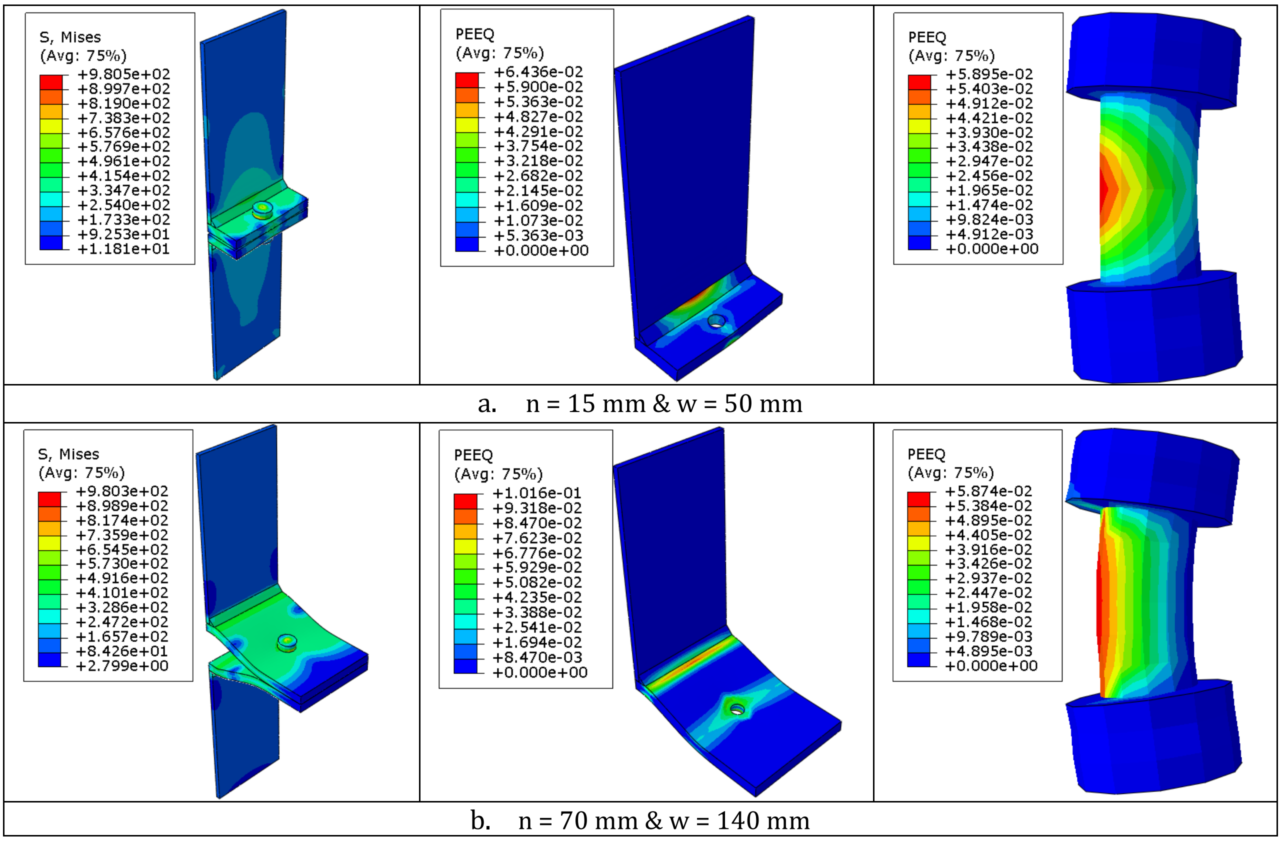

Fig. 13. Ultimate Stage of Specimens of t = 10 mm

With a flange thickness of 15 mm or 20 mm, the T-stubs failed by bolt fracture (Mode 3) for short gauge distances. Negligible deformation took place in the flanges. The bolt exhibited a straight shank at the end of the loading, corresponding to only tensile deformation (Fig. 14.a, Fig. 15.a). For larger values of gauge distances, specimens with a flange thickness of 15 mm exhibited a failure mode 2. A double curvature of the flange and bending of the bolt were observed despite being less pronounced than for thinner flanges. Additionally, yielding was observed at both the web-to-flange toe and bolt line regions (see Fig. 14.b). It can hence be said that the specimens failed in Mode 2 close to 1. With a thickness of 20 mm flanges, the yielding of the flange affected only the web-to-flange toe region. The flange and the bolt exhibited negligible flexural deformation (Fig. 15.b).

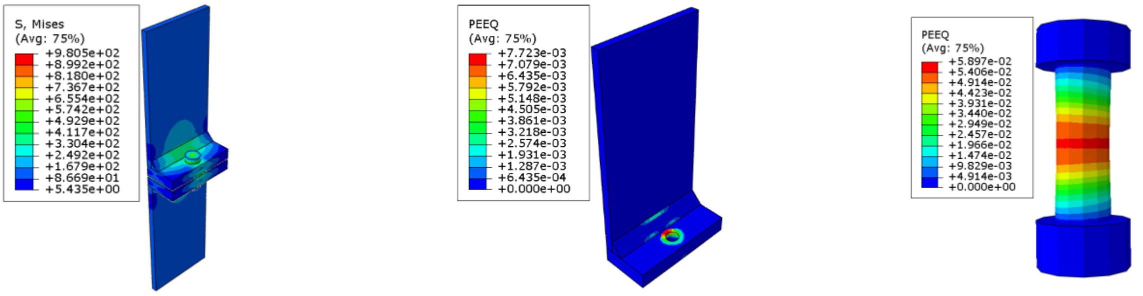

(a) n = 15 mm & w = 60 mm

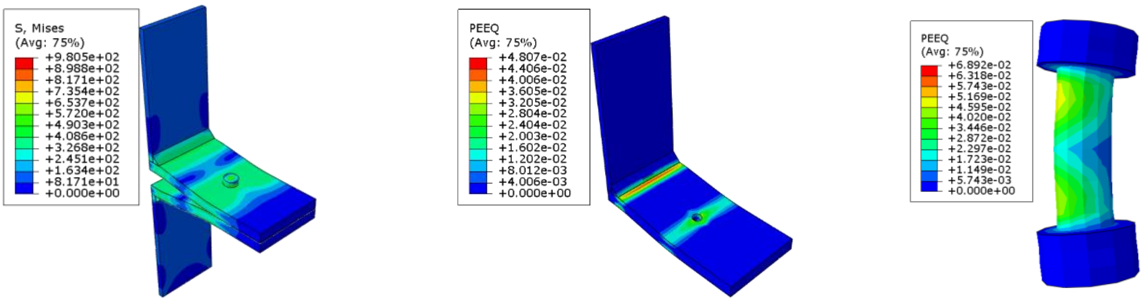

(b) n = 100 mm & w = 200 mm

Fig. 14. Ultimate Stage of Specimens of t = 15 mm

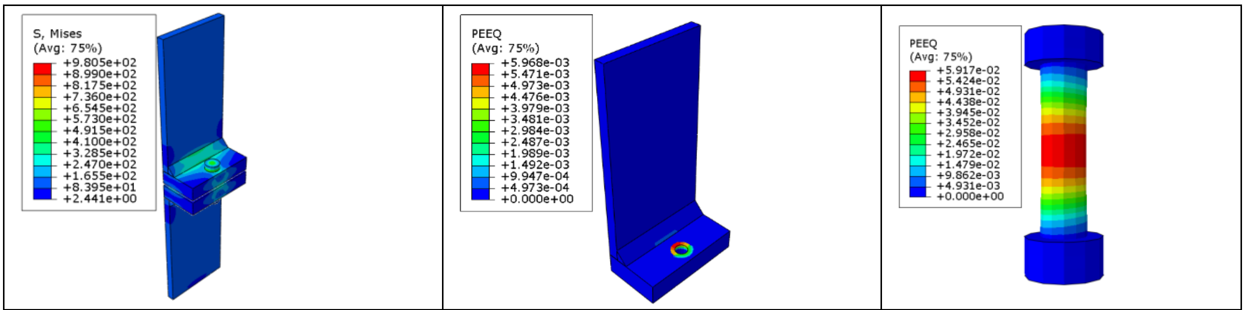

(a) n = 15 mm & w = 70 mm

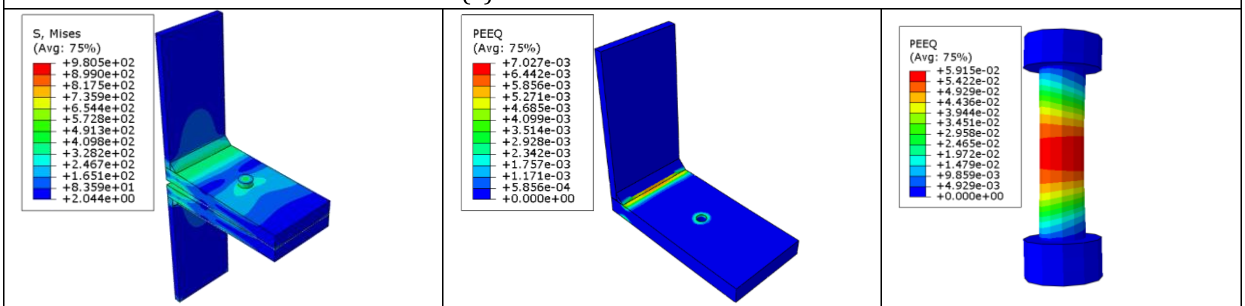

(b) n = 100 mm & w = 200 mm

Fig. 15. Ultimate Stage of Specimens of t = 20 mm

For the T-stubs that exhibited a failure of the bolt in addition to yielding at the web-to-flange toe region and bolt line region, the failure mechanism at the plastic resistance stage differed from the failure mechanism at the ultimate stage. When the plastic resistance is attained, yielding may be observed at the bolt line and the flange-to-web connection (failure mechanism 1). However, a reserve of resistance would allow the T-stub to continue deforming until the bolt fails, leading to a failure mechanism 2 (See Fig. 16).

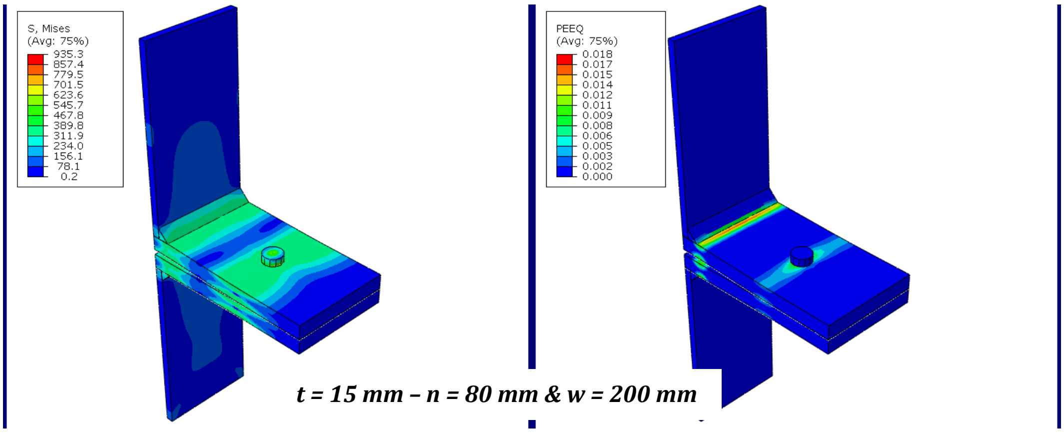

(a) Plastic Resistance Stage

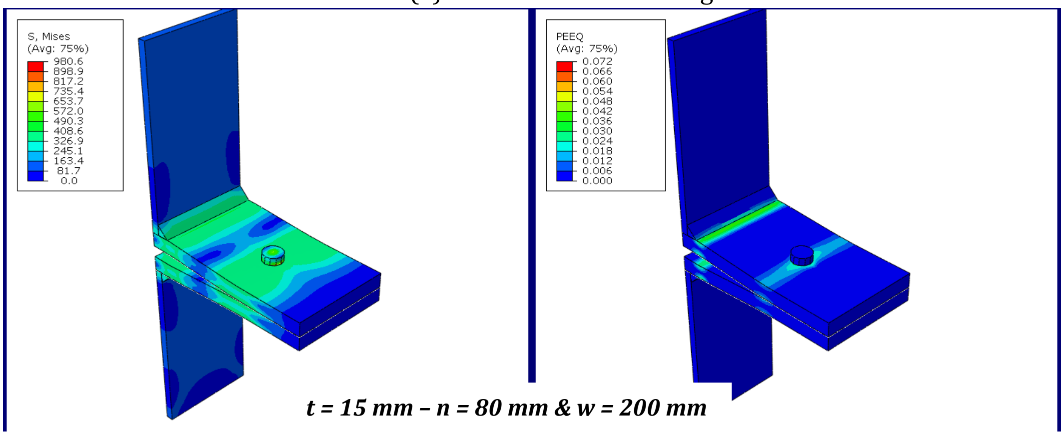

(b) Ultimate Stage

Fig. 16. T-stub with Two Different Failure Modes at (a) Plastic Resistance Stage and (b) Ultimate Stage

3.2. Plastic Resistance

Although plastic resistance was not the focus of this study, it was examined to obtain insight into the failure modes and the behavior of the flanges and the bolts when plastic resistance was reached. The plastic resistance of the T-stub (F_r) was set as the intersection between the two tangent lines of the load-displacement curve of the T-stubs at the initial and the final stages of the monotonic load (see Fig. 17.a). For a given edge distance, F_r decreased when the gauge distance was increased. Conversely to the gauge distance, as the edge distance was increased, the plastic resistance F_r is also increased. However, for high values of the gauge distance, there was a value of the edge distance for which the increased ratio of the plastic resistance in the function of the edge distance would be low. The influence of the edge distance and gauge distance on the plastic resistance is illustrated in Fig. 18. As for the flange thickness, it had a significant impact on the plastic resistance: an increase in thickness resulted in a higher resistance (see Fig. 19). For specimens exhibiting a failure mode 3, the resistance had a value of approximately 198 kN. This value corresponds to the tensile resistance of the bolts, which can be assessed using eq. (1) and (2).

$$F_r = \sum F_{tb} \qquad (1) \qquad\qquad F_{tb} = A_b . f_{ub} \qquad (2)$$

A_b is the cross-sectional area of the bolt. In general, the tensile stress area A_s is used but in our case the nominal gross area was used. f_{ub} is the ultimate tensile strength of the bolt.

It is worth noting that the rate of change in the plastic resistance was higher in the case of thickness or gauge distance variation.

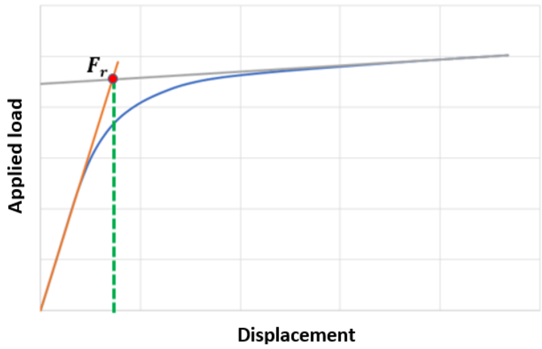

(a)

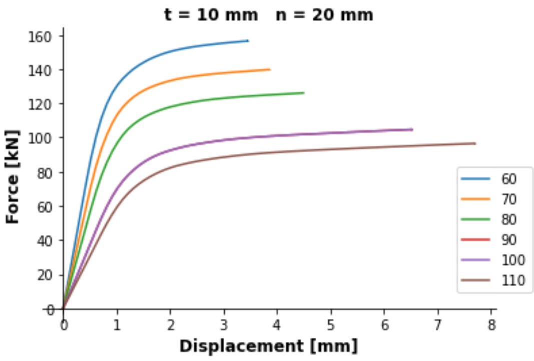

(b)

Fig. 17. Plastic Resistance and F-D Curves for Different Values of w for t = 10 mm & n = 20 mm

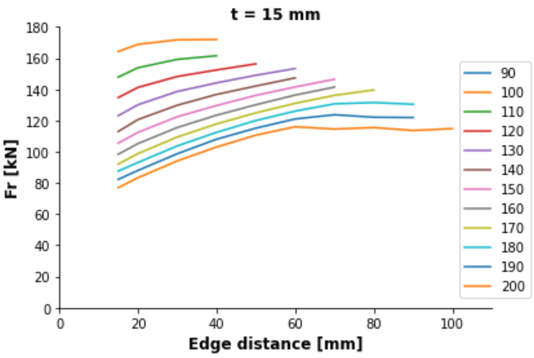

(a)

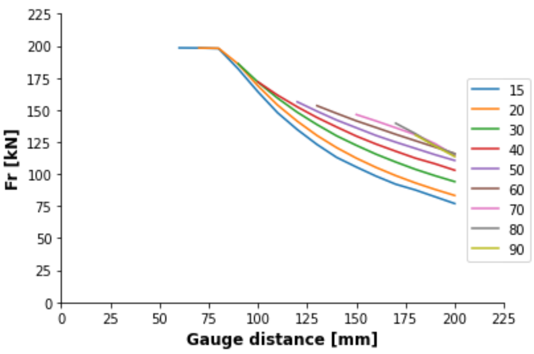

(b)

Fig. 18. Variation of the T-stub Resistance in function of n and w for t = 15 mm

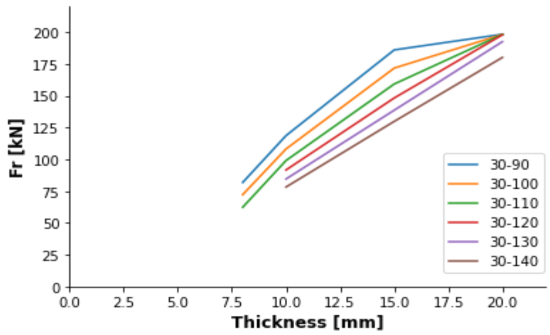

(a) n = 30 mm

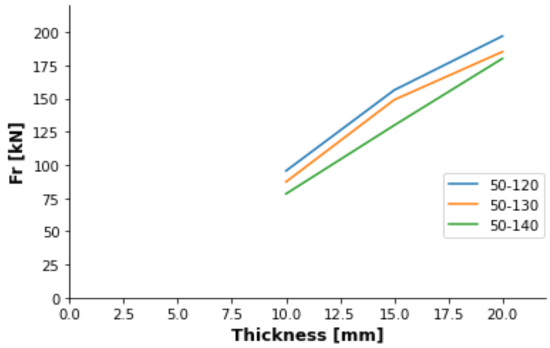

(b) n = 50 mm

Fig. 19. Variation of the Resistance in function of the Flange Thickness for Different n-w Combinations

Furthermore, as depicted in Fig. 20 and Fig. 21, it can be seen that the resistance F_{EC3}, predicted by Eurocode 3 formulation and using the experimental material properties, was lower than the numerical plastic resistance F_r; showing that the Eurocode predictions are conservative. The ratio between the predicted and the numerical plastic resistances ranged from 1.15 to 1.38 for a flange thickness of 8 mm and 1.3 to 1.47 for a flange thickness of 10 mm. With t = 15 mm and t = 20 mm, the ratio ranged from 1.3 to 1.63 to 1.28 to 1.63. A ratio of 1.63 was found common to all the specimens involving a mode three failure.

3.3. Prying Effect in the Bolt

The effects of prying can be evaluated by examining the induced prying force Q, the total bolt force B and the moment in the bolts M. Two situations were considered: the values corresponding to the attainment of the plastic T-stub resistance and the maximum values.

3.3.1. Prying Force

The difference between the total bolt force B and the applied load expresses the prying force Q arising in the bolt.

$$Q = B - F \quad (3)$$

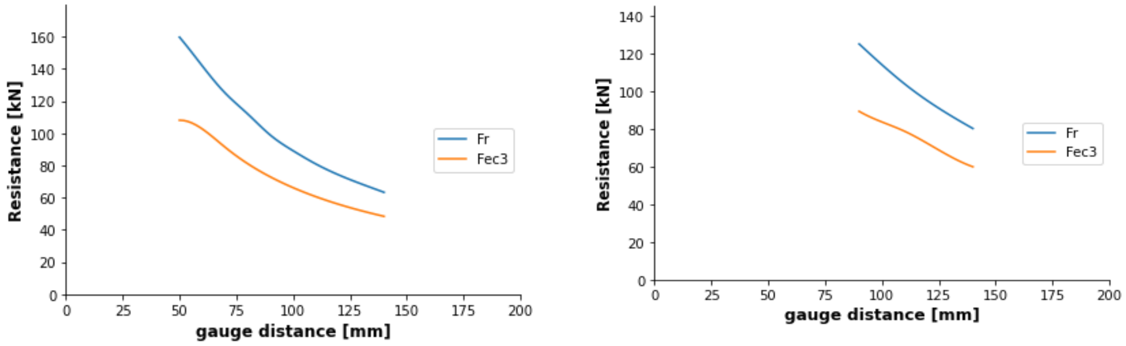

(a) n = 15 mm (b) n = 40 mm

Fig. 20. Variation of F_r and F_{ec3} in function of the Gauge Distance for t = 10 mm

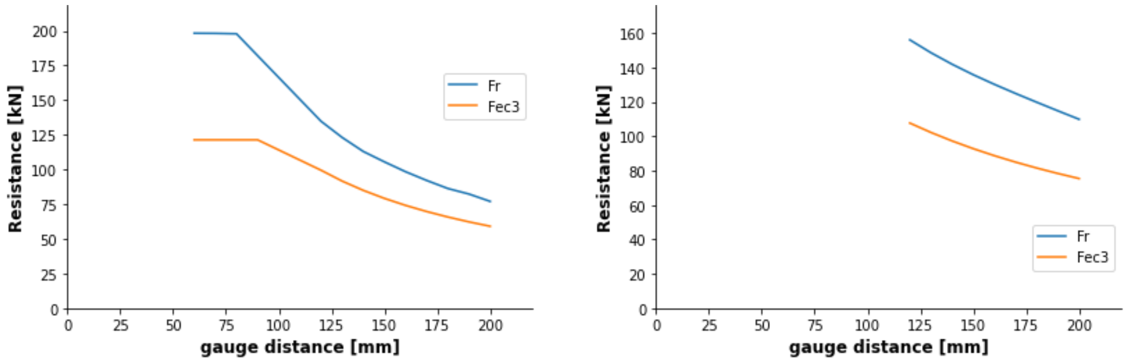

(a) n = 15 mm (b) n = 50 mm

Fig. 21. Variation of F_r and F_{ec3} in function of the Gauge Distance for t = 15 mm

Prying action, especially prying force, has long been considered related to contact phenomena. The average contact stress distribution between the connected parts induces prying forces. In the case of non-preload bolts, the prying forces can be obtained by the integral of the normal stress distribution over the contact zone (Couchaux et al., 2017). The prying forces, assessed by using eq. (3), were compared to the force-resultant (CF2) of the contact stresses throughout the loading. As illustrated in Fig. 22, the graphs coincide.

An increase in the gauge distance for all the specimens increased the prying force, as observed in previous studies (Swanson and Leon, 2000; Girão Coelho, 2004). The deformability of the T-stub flange is correlated to the gauge distance. A flange with a longer gauge distance will deform more. The deformation of the flange will induce contact stresses between the flanges, causing prying forces.

The observations reported by Nair et al. (1969) show an optimum value for the edge distance. For values of n below the optimum value, increasing the edge distance increased the prying forces. Beyond the optimum value, prying forces decrease as the edge distance increases. This trend is more noticeable for specimens involved in failure Mode 3 (the specimens with a flange thickness of 20 mm or specimens with a flange thickness of 15 mm and low values of the gauge distance). With specimens involved in failure Mode 2 or Mode 1, only a decrease in the prying forces was observed as the edge distance was increased.

The variations of prying force in the function of the edge distance and the gauge distance are illustrated in Fig. 23-26. The prying forces at the attainment of the plastic T-stub resistance Q_r and the maximum prying force, Q_{max} were considered.

An increase in the flange thickness expectedly resulted in a substantial decrease in the prying force (See Fig. 27). When the flange thickness increases, the rigidity of the flange increases substantially. Consequently, the flanges are less deformable, and less contact stresses develop

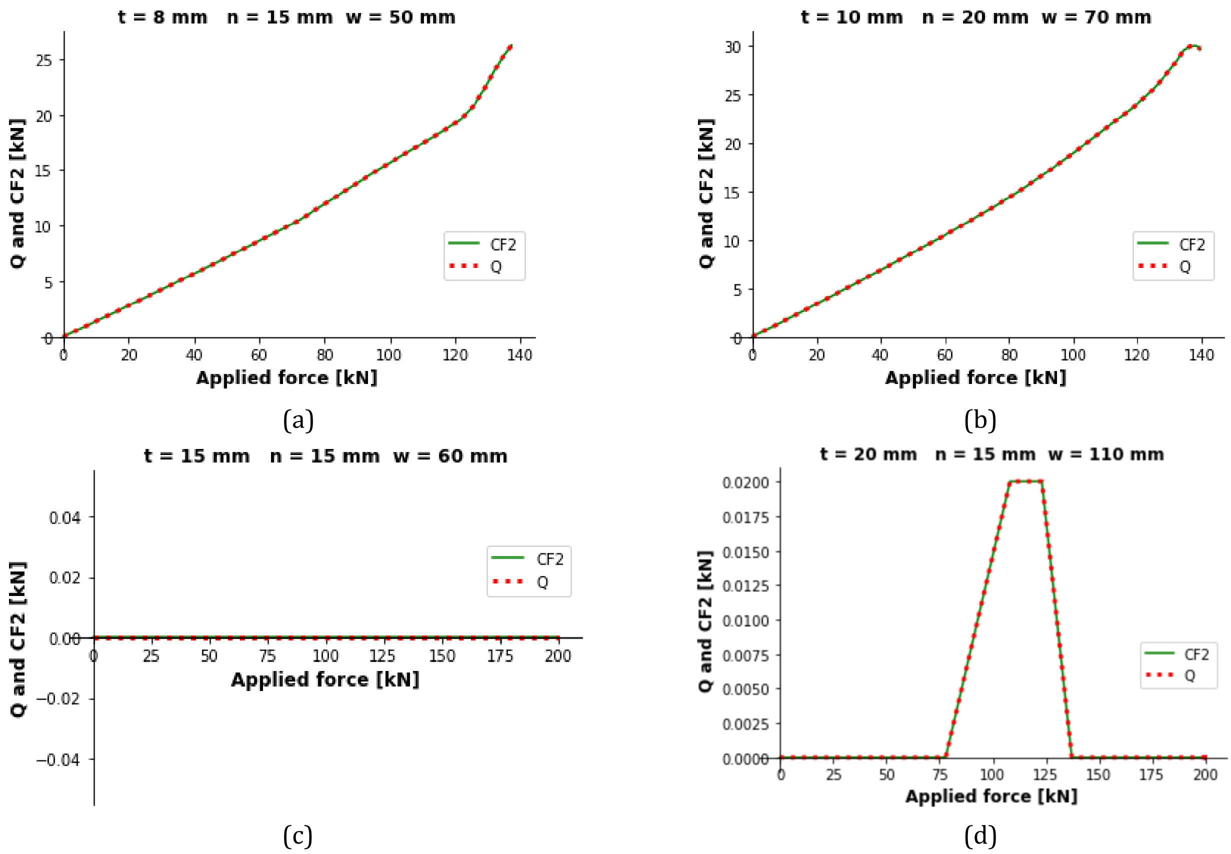

Fig. 22. Prying Forces and Force-resultant of the Contact Stresses

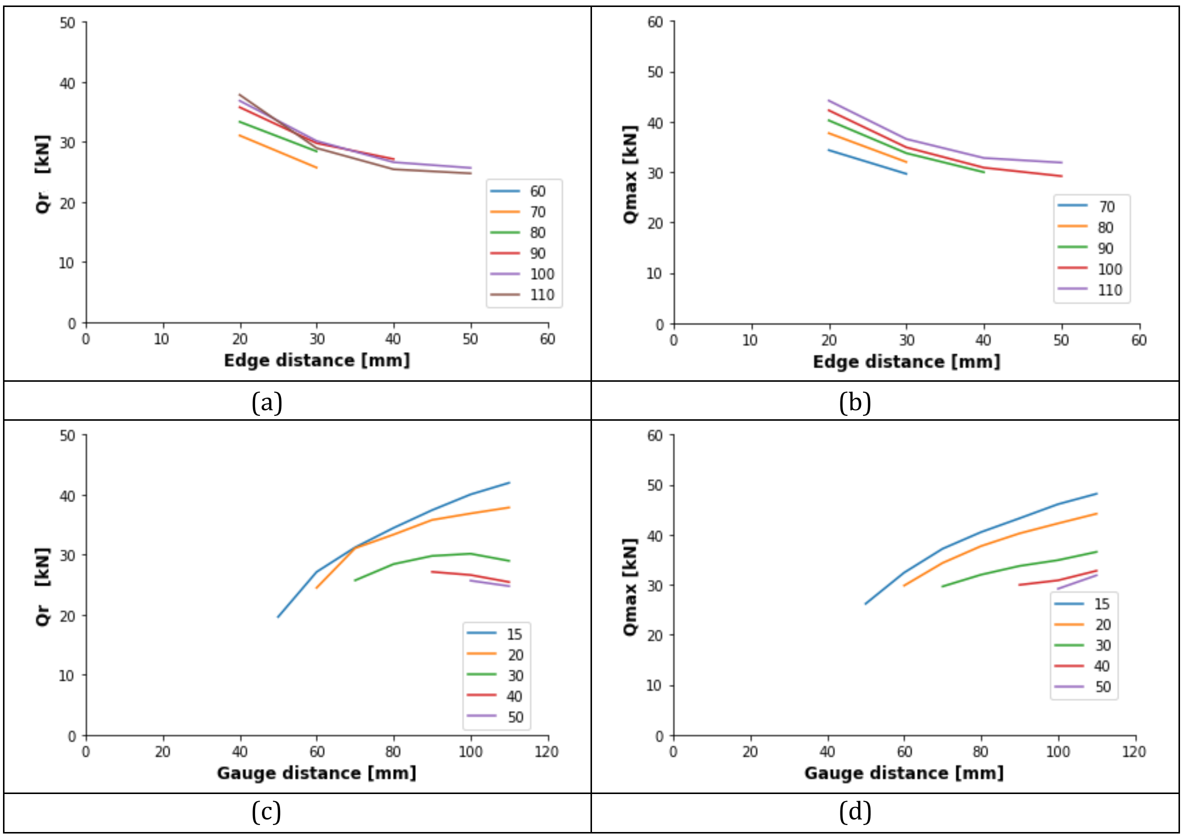

Fig. 23. Variation of Prying Force in function of the Edge Distance and the Gauge Distance for t = 8 mm

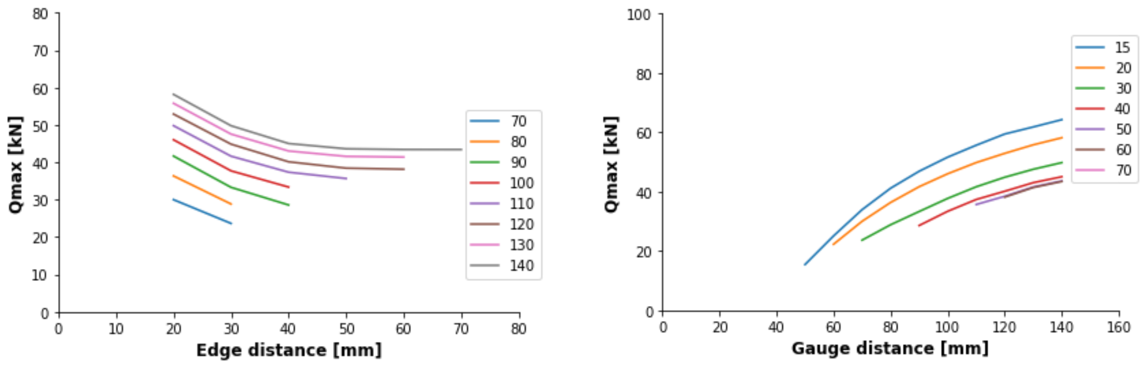

(a) (b)

Fig. 24. Variation of Prying Force in function of the Edge Distance and the Gauge Distance for t = 10 mm

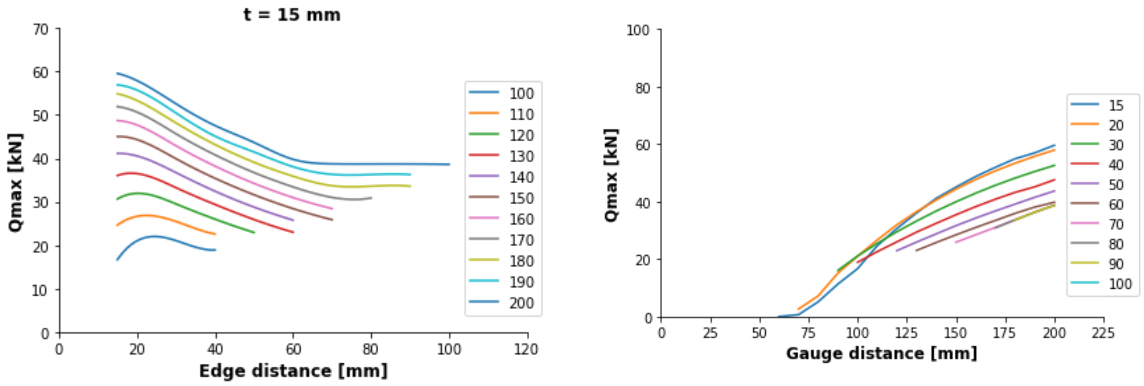

(a) (b)

Fig. 25. Variation of Prying Force in function of the Edge Distance and the Gauge Distance for t = 15 mm

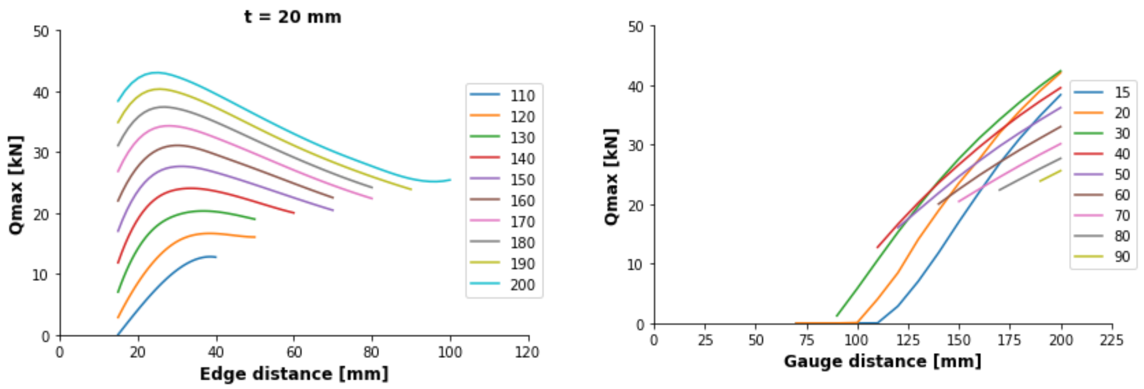

(a) (b)

Fig. 26. Variation of Prying Force in function of the Edge Distance and the Gauge Distance for t = 20 mm

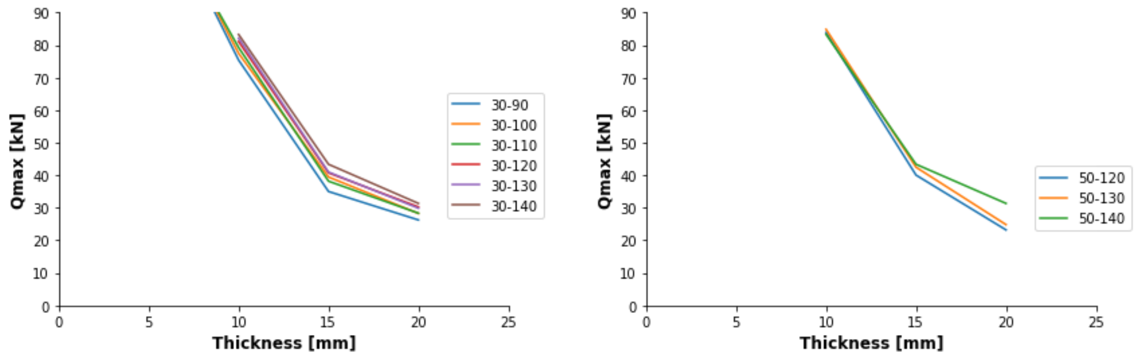

(a) n = 30 mm (b) n = 50 mm

Fig. 27. Variation of the Qmax in function of the Flange Thickness for Different n-w Combinations

For each thickness, the maximum values of prying force were found in specimens with the smallest value of n/m (corresponding to a combination of the highest value of w and the smallest value of n). The dimension m, illustrated in Fig. 28, is the distance between the bolt axis and the plastic hinge arising near the web.

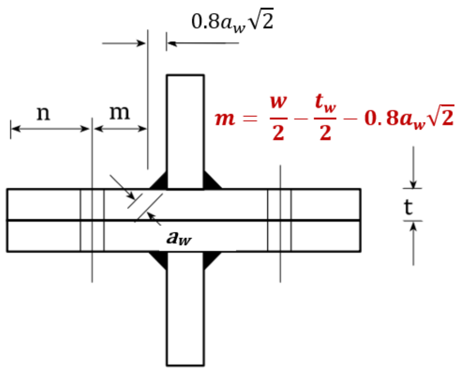

Fig. 28. Distance between the Bolt Axis and the Plastic Hinge Arising near the Web

With thicker flanges (15 mm and 20 mm), zero or negligible prying (less than 10% of the ultimate axial resistance of the bolt) was observed in some specimens. The specimens were all involved in a failure mode 3. In the case of zero prying throughout the loading, the deformation of the flanges was negligible compared to the elongation of the bolt. As the gauge distance increases, although small, the deformation of the flanges is enough to induce contact in the early stages of the loading. However, as the load increases, the bolt elongation exceeds the flange deformation, leading to a loss of contact between the connected members.

Considering that prying forces are equivalent to the resultant of the contact stresses, it was deemed essential to examine the position of the resultant. Two directions were considered: X-direction and Z-direction. The center of the force due to contact pressure in the Z-direction is labeled XN3, and the center of the force due to contact pressure in the X-direction is labeled XN1.

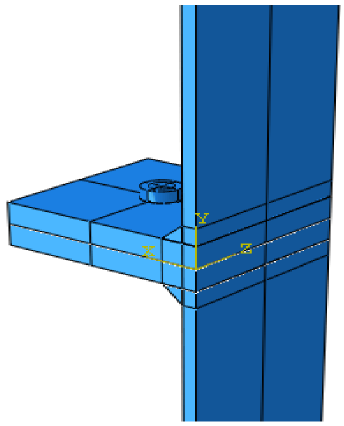

Fig. 29. Location of the Origin

Considering the variations of XN1 throughout the loading, three cases were observed:

- Case 1: no contact throughout the loading (See Fig. 30.a, Fig.30.b)
- Case 2: initial contact followed by a loss of contact (See Fig. 30.c, Fig.30.d)
- Case 3: the connected elements remained in contact throughout the loading. This was the case for most specimens. (See Fig. 30.e, Fig.30.f)

For all the specimens, throughout the loading, XN3 is located approximately at 50 mm = b/2 from the origin (See Fig. 31), indicating the symmetry of the contact stresses in the Z-direction.

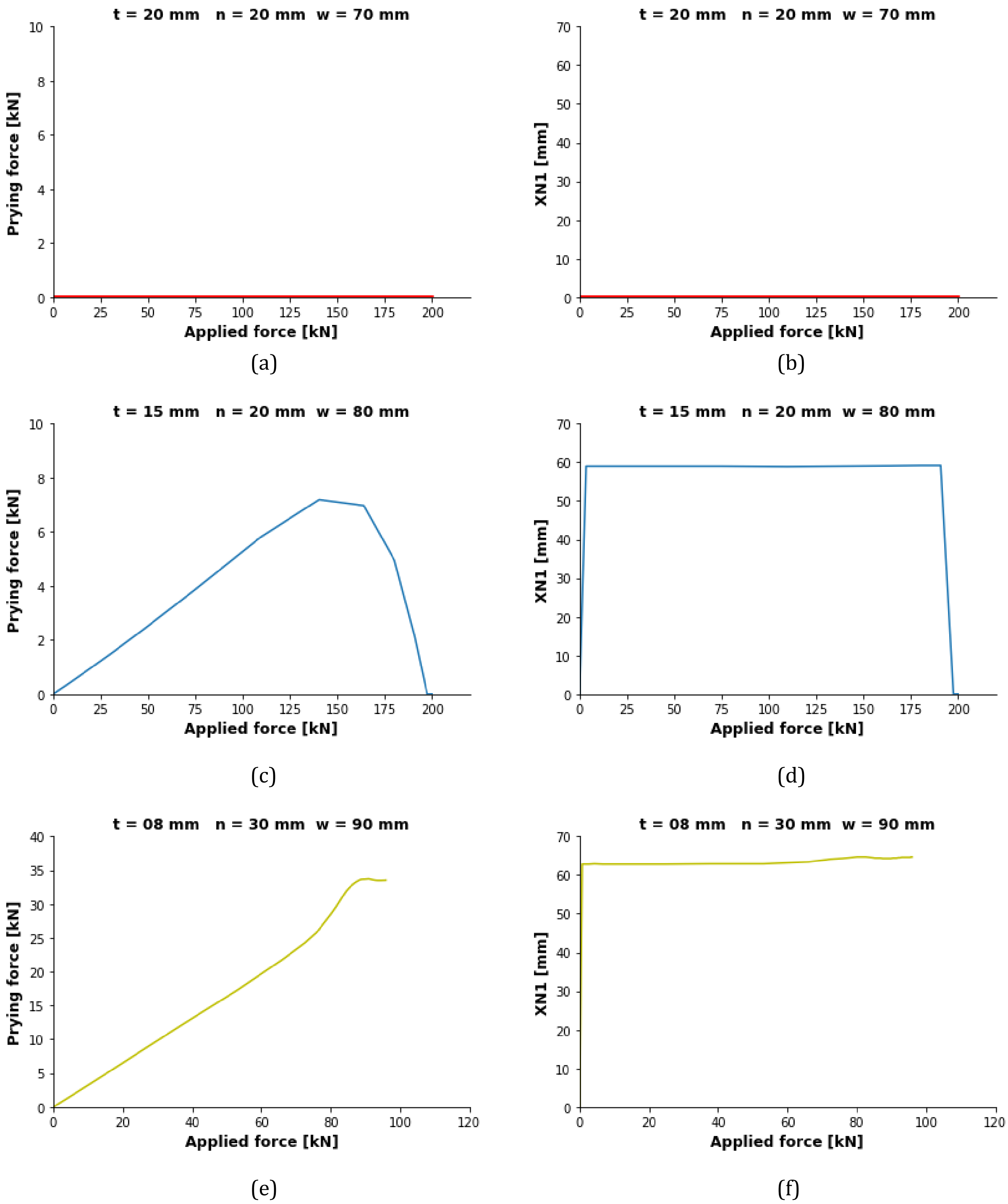

Fig. 30. Variation of the Prying Force and XN1 throughout the Loading for Different Cases

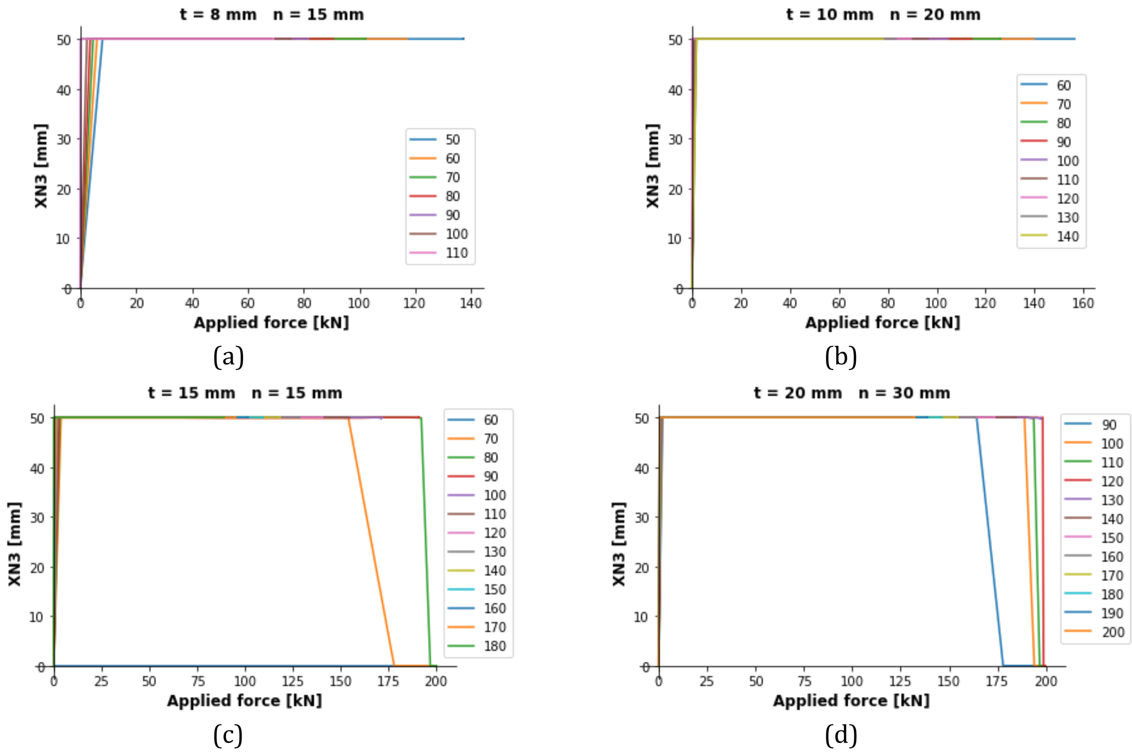

Fig. 31. Variations of XN3 throughout the Loading

The center of the forces due to contact pressure in the X-direction varied throughout the loading, indicating an evolution of the contact pressure. Two stages were considered and compared: attaining the T-stub plastic resistance and the ultimate stage. As depicted in Fig. 32, the values were similar or had little difference. It could be inferred that the position of the resultant contact stresses is not dependent on the loading in the case of non-preload bolts.

For the same edge distance, the position of the resultant in the X-direction, calculated according to the tip of the flange, did not exhibit much variation as the gauge distance increased (See Fig. 33). Nevertheless, the resultant moved farther from the tip as the edge distance increased; meaning that the position of the resultant depends on the edge distance.

3.3.2. Total Bolt Force

Conversely to the prying force, the total bolt force B increased as the gauge distance was increased. As mentioned in the previous sections, an increase in the gauge distance resulted in a decrease in the resistance of the T-stubs and an increase in the prying force. The decrease ratio of the resistance is greater than the increase ratio of Q per Eq. (3), leading to a decrease in the total bolt force.

Concerning the variations in function of the edge distance, a decreasing pattern was observed for specimens involving thinner flanges (8 mm and 10 mm). In contrast, the opposite was observed for $t = 15\ mm$ and $t = 20\ mm$. Furthermore, for a thinner flange, the variations of B_{max} are more distinct from one another than those for thicker flanges (Fig. 34). The highest values of the total bolt force corresponded to specimens combining the smallest values of both w and n. With thinner flanges, the total bolt force decreases as the edge distance increases. A similar variation is observed with the gauge distance. However, as illustrated in Fig. 35, in specimens with thicker flanges (15 mm and 20 mm), a linear relationship can be assumed between B_{max} and the gauge distance, as well as the edge distance. Moreover, the variations of B_{max} can be approximated by a single line, showing that the maximum total bolt force is not dependent on the edge and gauge distances when thicker flanges are used. Since the failure of the specimens involved the failure of the bolts, the maximum total bolt force, equivalent to the total bolt force at the ultimate stage, is more dependent on the bolt characteristics than the flange characteristics. In some specimens that failed in Mode 1, the maximum bolt force was as low as 77 kN, which is relatively small compared to the ultimate bolt resistance.

The variations of the maximum bolt force in function of the flange thickness are illustrated in Fig. 36.

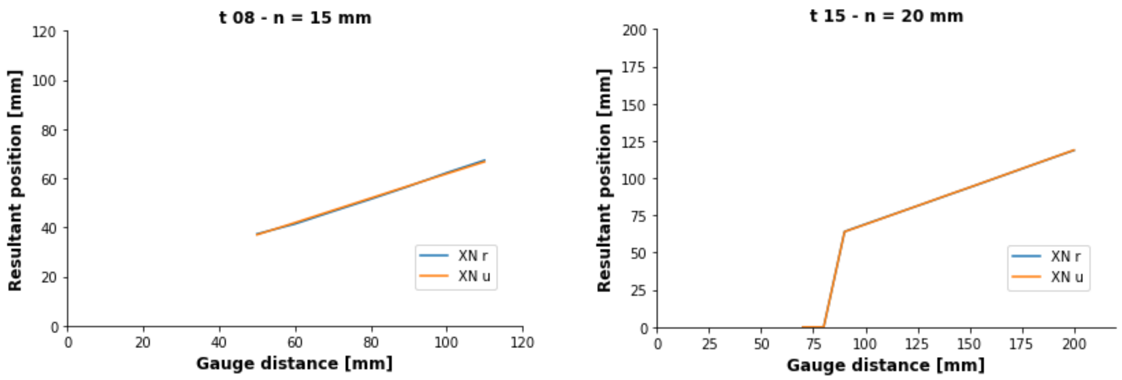

(a) (b)

Fig. 32. XN1 at the Attainment of the Plastic Resistance and the Ultimate Stage

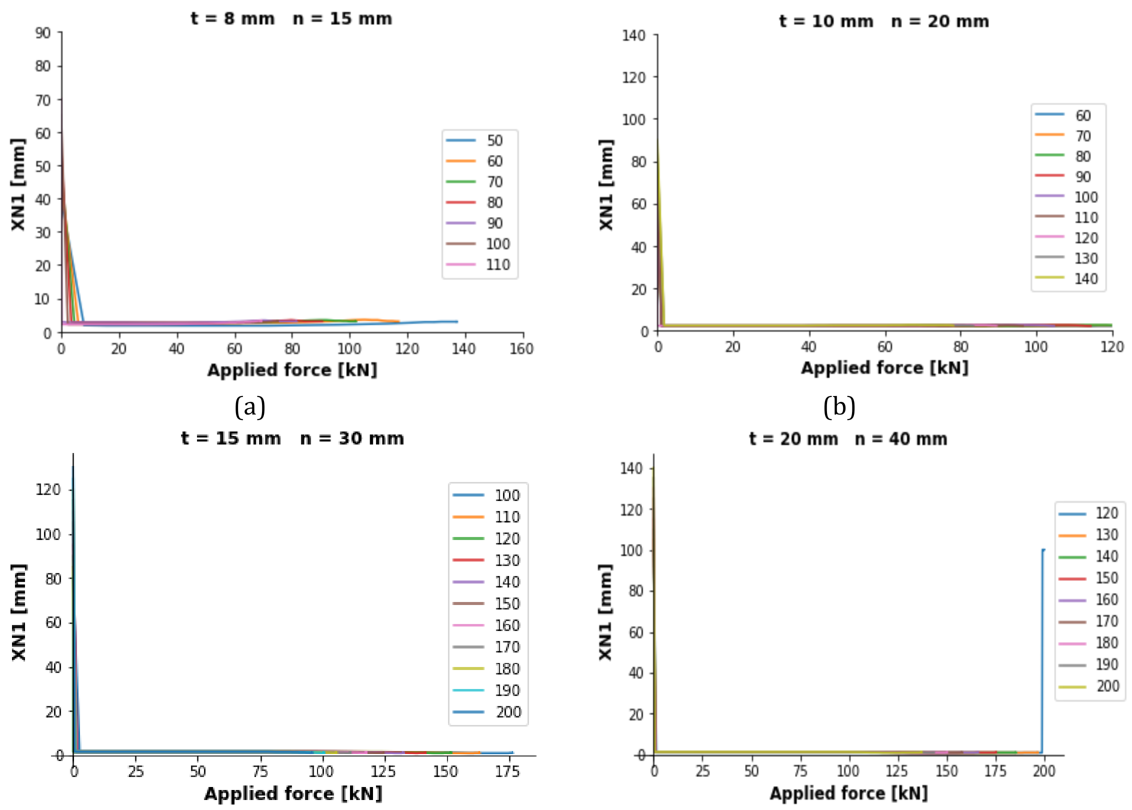

(a) (b)

(c) (d)

Fig. 33. Position of the Resultant of the Contact Stresses in the X-direction.

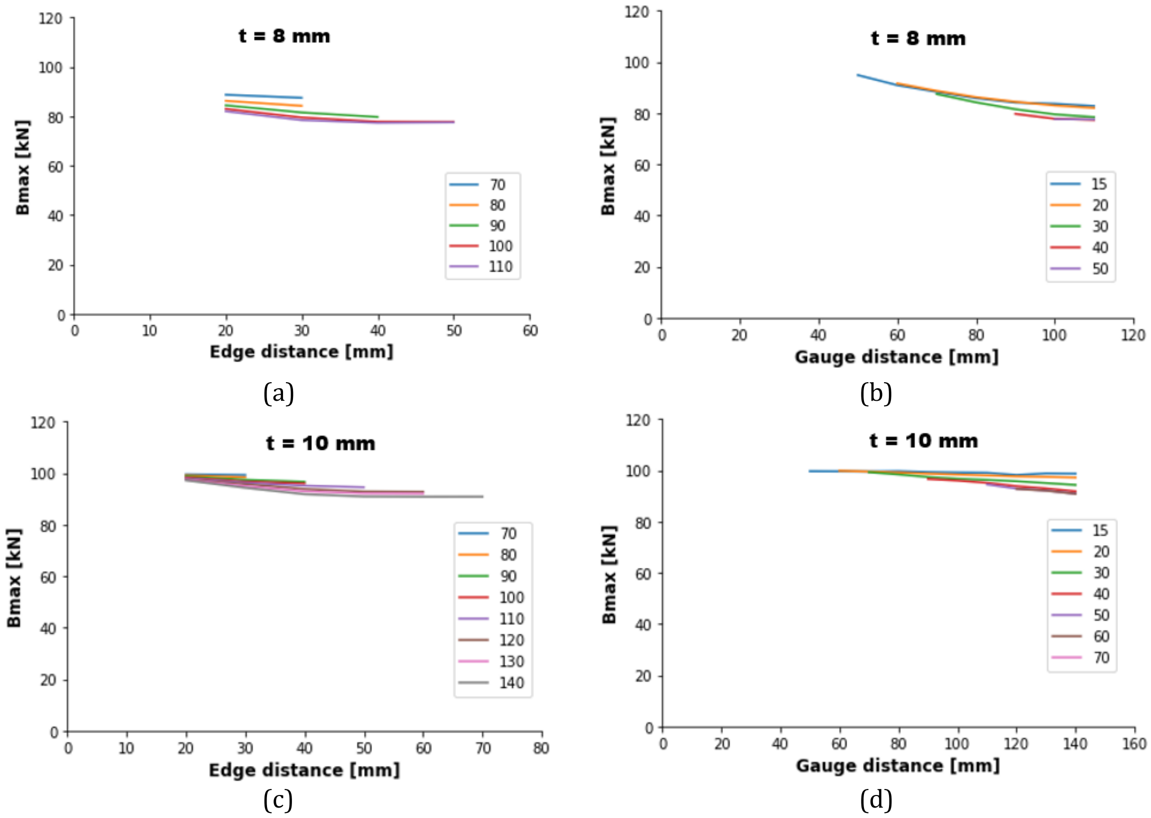

Fig. 34. Variation of the Total Bolt Force in function of n and w for t = 8 mm and t = 10 mm

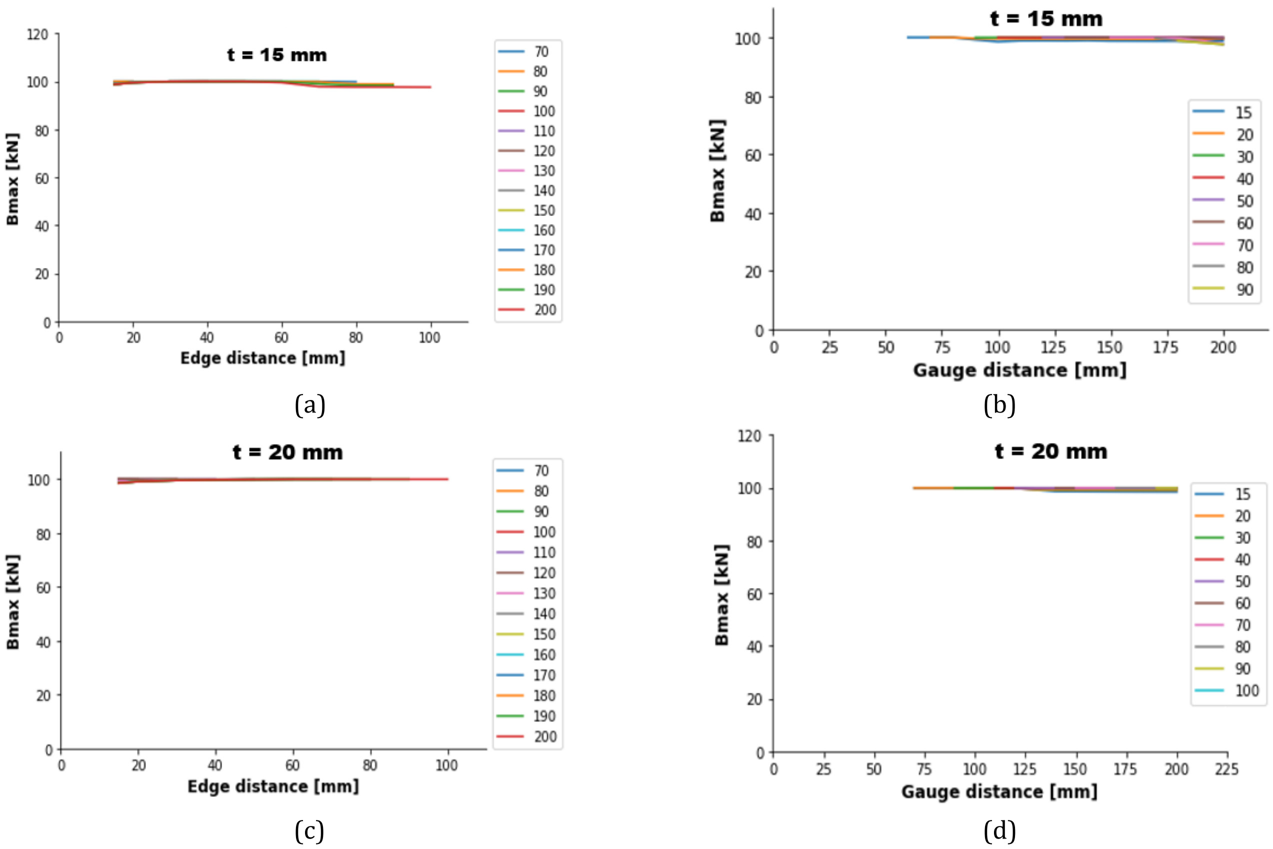

Fig. 35. Variation of the Total Bolt Force in function of n and w for t = 15 mm and t = 20 mm

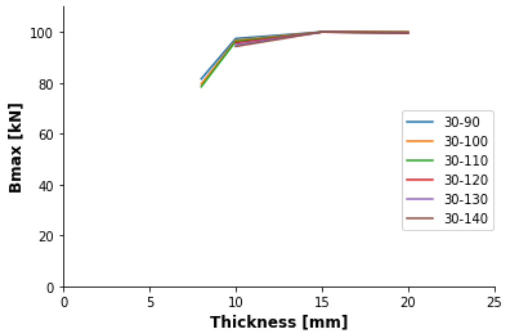

(a) n = 30 mm

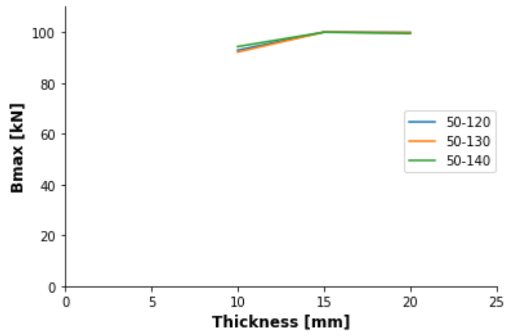

(b) n = 50 mm

Fig. 36. Variation of B_{max} in function of the Flange Thickness for Different n-w Combinations

3.3.3. Bolt Moment

The moment in the bolts is induced by the deformation of the flanges, which subjects the bolts to flexural deformation. Even in specimens that exhibited zero prying force, the moment in the bolts was present throughout the loading. Unlike the prying force, which is related to contact stresses, the bolt moment is related to the rigidity of the flanges and the bolts. In other words, the moment in the bolts is strongly dependent on both the flanges' deformability and the bolts' deformability.

For all the specimens, the moment in the bolt exhibited the same variation throughout the loading: as the applied load increases, the bolt moment increases until a maximum value. Beyond that point, the bolt moment decreases as the applied load increases until the ultimate load (See Fig. 37). In T-stubs with thinner flanges (8 mm and 10 mm), despite being much lower than M_{max}, the moment at the ultimate stage was still positive (Fig. 37.a, Fig. 37.b). The positive sign of moment indicated that the flange continued to deform, subjecting the bolt to a bending (failure mode involving the yielding of the flange). However, only a few specimens presented ultimate positive moments for t = 15 mm and t = 20 mm. In most specimens, the ultimate moment was negative (See Fig. 37.c, Fig. 37.d). Considering that the flanges possess a relatively higher rigidity than the bolts, after the separation of the flanges, a further increase in the applied load would only result in a tension of the bolts; which would tend to cancel the bending that previously occurred in the bolt due to the flange deformation. It is worth mentioning that, with thicker flanges, the ultimate moment (positive or negative) was negligible enough to be considered equal to zero.

The variations of the bolt moment were similar to that of the prying force vis-à-vis the gauge distance. For all the specimens, the increase in the gauge distance increased in bolt moments (See Fig. 38 and Fig. 39). Considering a certain edge distance, the rigidity of the flanges decreases, and the deformability increases as the gauge distance increases. The flanges' deformation then subjects the bolts to flexural action. However, the bolt moment variations in the edge distance function are different in specimens with thinner flanges (8 mm and 10 mm) and specimens with thicker flanges (15 mm and 20 mm). With thinner flanges, the moment in the bolt increases as the edge distance increases (See Fig. 38 and Fig. 39). It should also be noted that the influence of the edge distance is lower for high values. Similarly to the prying forces, an increase in the thickness resulted in lower bending moments in the bolts (See Fig. 40).

The ultimate flexural resistance of the bolt M_{ub} computed using equations (4) was 156 kN.mm. With 8 mm, 10 mm, 15 mm and 20 mm flange thicknesses, the maximum bolt moments attained were respectively 65%, 55%, 41%, and 37% of the M_{ub} (See Table 5). The moment in the bolts can reach proportions significant enough for the combined tensile and flexural action to yield considerable stresses in the bolt. On that account, the bolt moment has to be considered in the design.

$$M_{ub} = \frac{I}{\emptyset_b/2} \cdot f_{ub} \tag{4}$$

Where I is the second moment of inertia, $\emptyset_b$ the bolt diameter, and f_{ub} the ultimate stress of the bolt.

Table 5. Maximum Bolt Moment and their Ratios to Ultimate Bolt Flexural Resistance

Thickness	M_{max}	M_{max}/M_{ub}
8 mm	101.2 kN.mm	0.65
10 mm	86.5 kN.mm	0.55
15 mm	64.1 kN.mm	0.41
20 mm	58.5 kN.mm	0.38

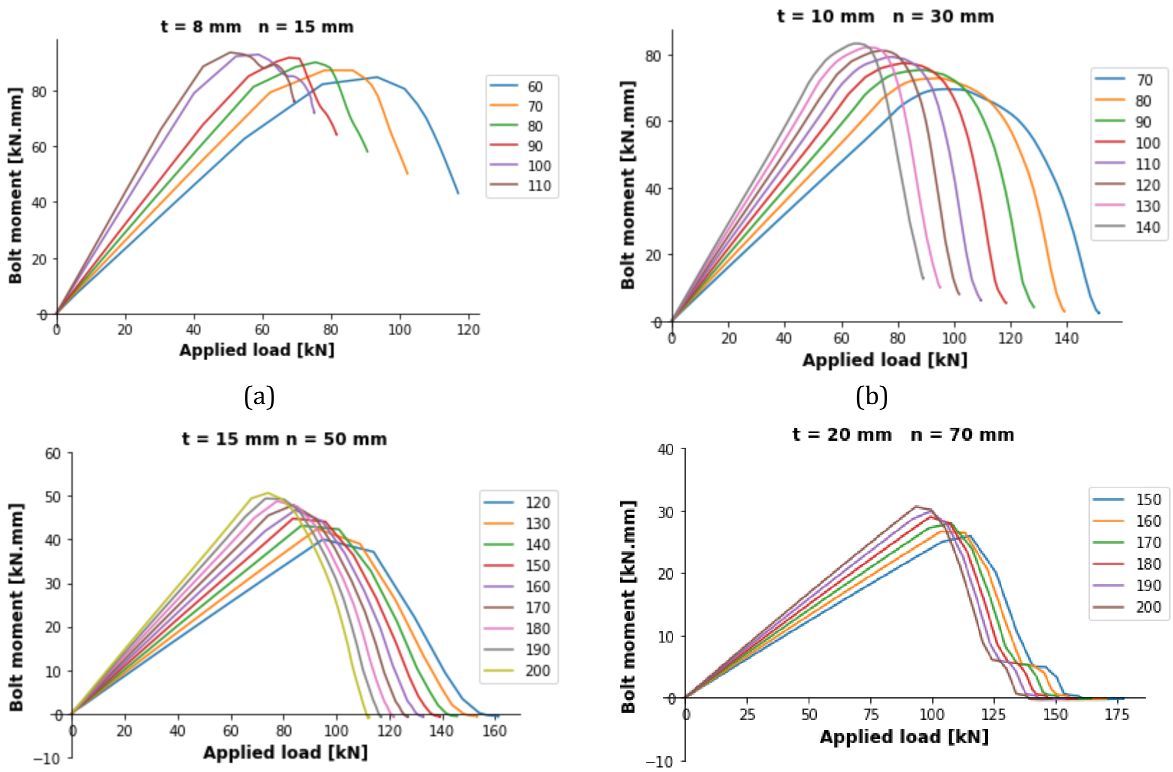

(a) (b)

(c) (d)

Fig. 37. Variations of the Bolt Moment throughout the Loading

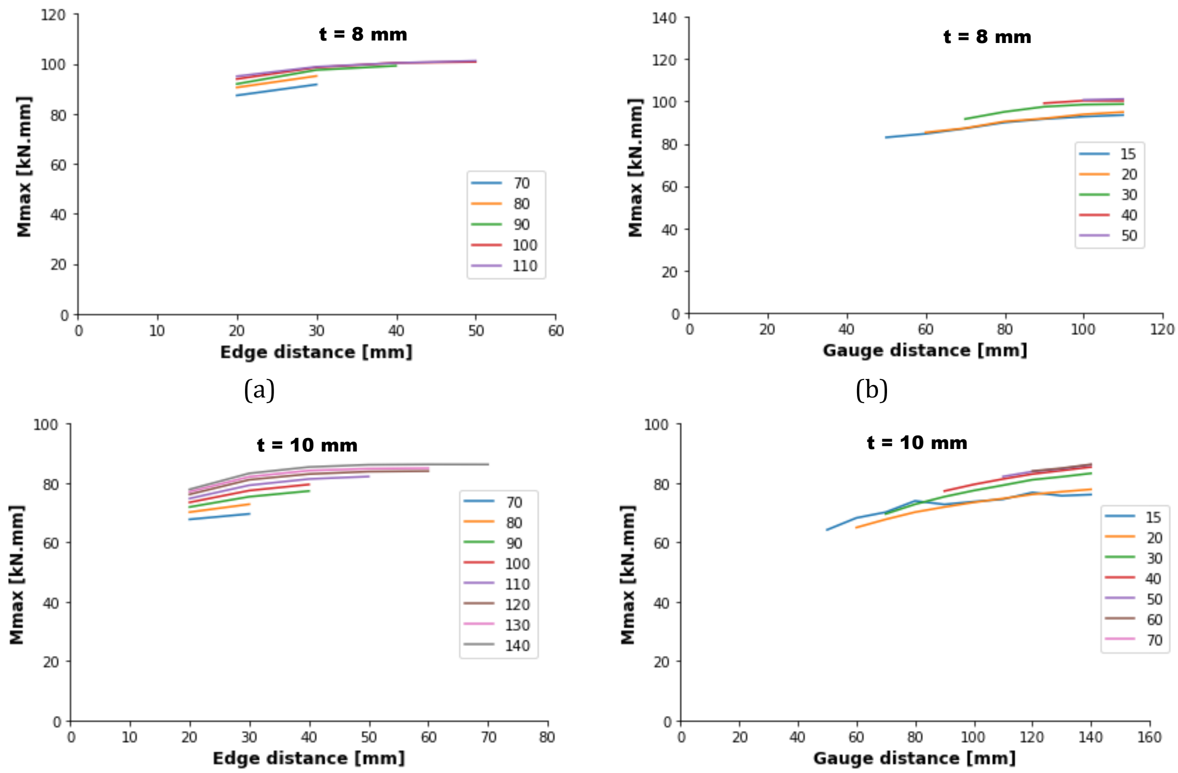

(a) (b)

(c) (d)

Fig. 38. Variations of the Maximum Bolt Moment in function of n and w for t = 8 mm and t = 10 mm

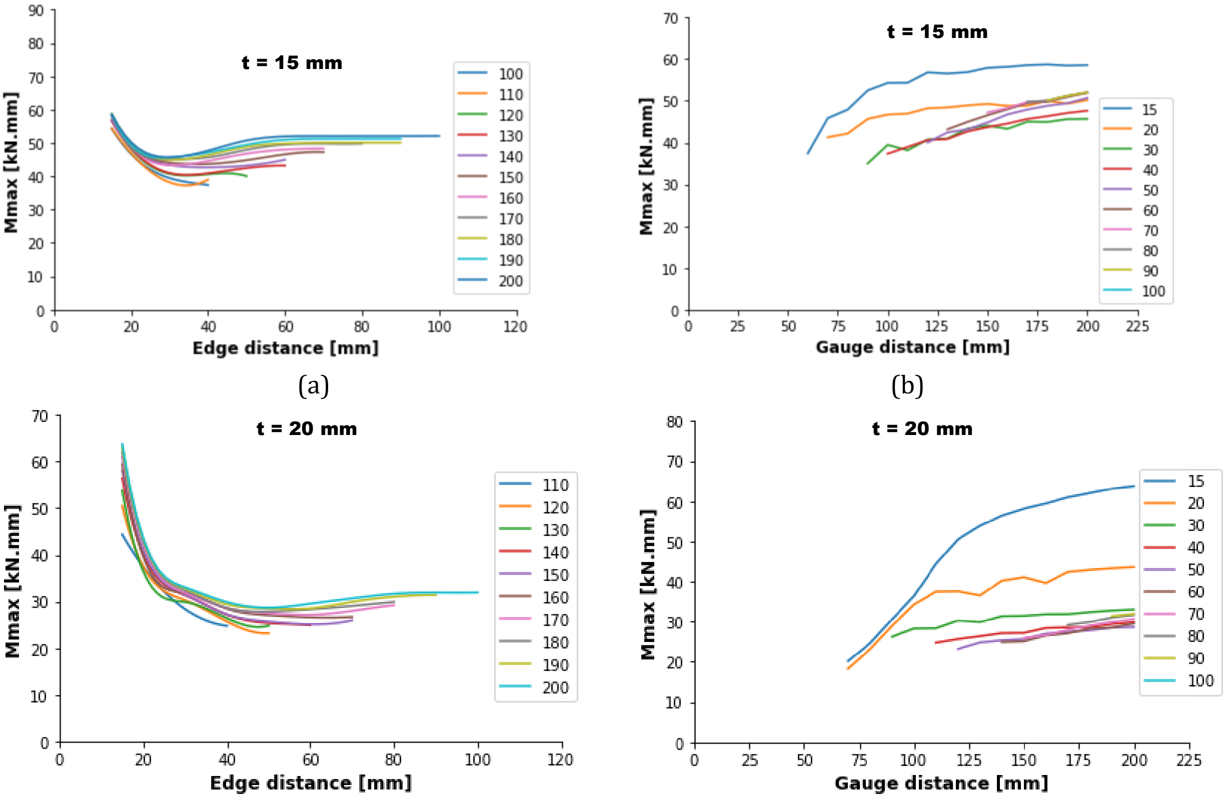

(a) (b) (c) (d)

Fig. 39. Variations of the Maximum Bolt Moment in function of n and w for t = 15 mm and t = 20 mm

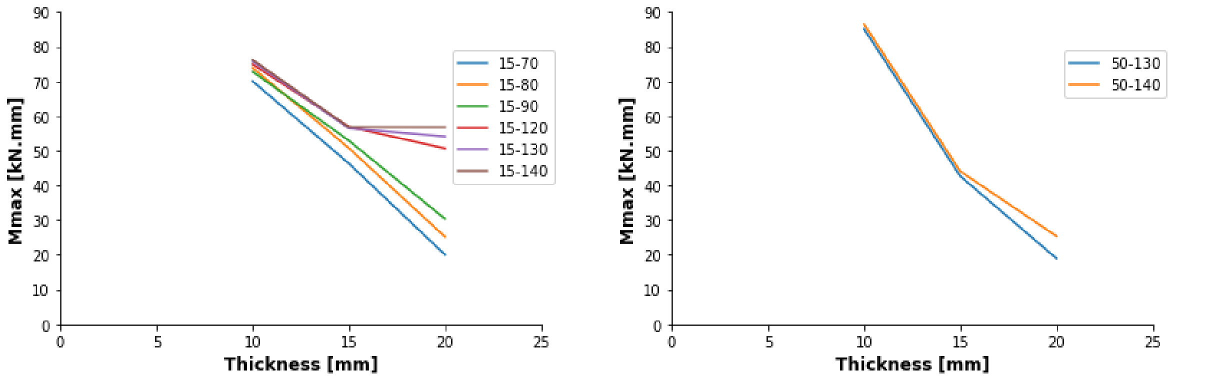

(a) **n = 15 mm** (b) **n = 50 mm**

Fig. 40. Variation of the Maximum Bolt Moment in function of the Flange Thickness for Different n-w Combinations

3.3.4. M-N Interactions Curves

By comparing the prying force Q, the total bolt force B and the total bolt moment M for each increment to their respective maximum values, it was observed that for all the specimens, the maximum moment M_{max} was always reached before Q_{max} and B_{max} were reached. For all the models, B_{max} corresponded to the total bolt force at the ultimate load. However, Q_{max} and M_{max} where different from the prying force and bolt moment values at ultimate stage. Concerning prying force, in some specimens the Q_{max} and the prying force at ultimate load coincided. The specimens failed in Mode 1 or Mode 2 close to 1. For specimens with a thinner flange, the maximum values of Q and B were reached almost at the same load. However, when thicker flanges were used, for short gauge distances, Q_{max} was attained for loads much lower than that of B_{max}. As the gauge distance was increased, the load of attainment of Q_{max} got closer to a load of attainment of B_{max} (see Fig. 41).

Considering that the bolts are subjected to the combined action of flexure and tension, it appeared important to analyze the M-N interaction curves of the T-stubs. As illustrated in Fig. 42, the maximum and ultimate bolt moment increases as the gauge distance increases. This is compatible with the fact that the deformability of the flange increases with the function of the gauge distance. Conversely, the maximum total force in the bolts – equivalent to the ultimate total bolt force - decreases as the gauge distance increases. With thicker flanges, the maximum total bolt force is practically the same in all the specimens. This is because the failure of these specimens involves the failure of the bolts.

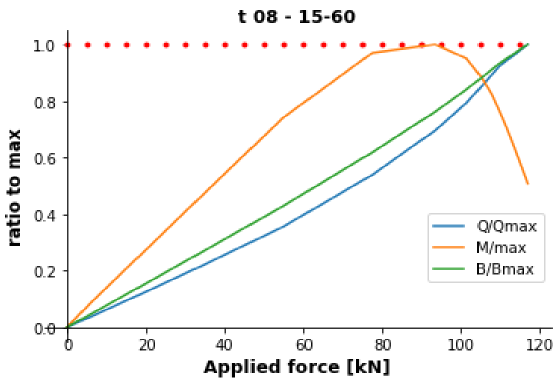

(a) t = 8 mm - n = 15 mm – w = 60 mm

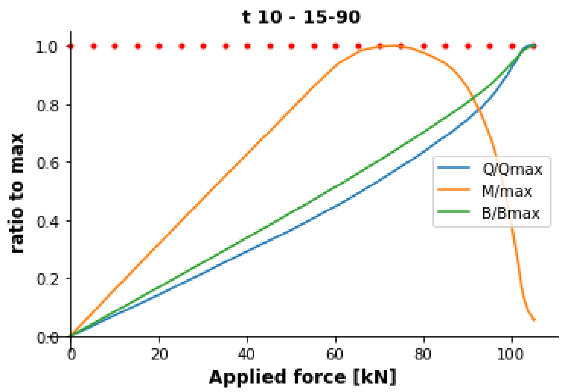

(b) t = 10 mm - n = 15 mm – w = 90 mm

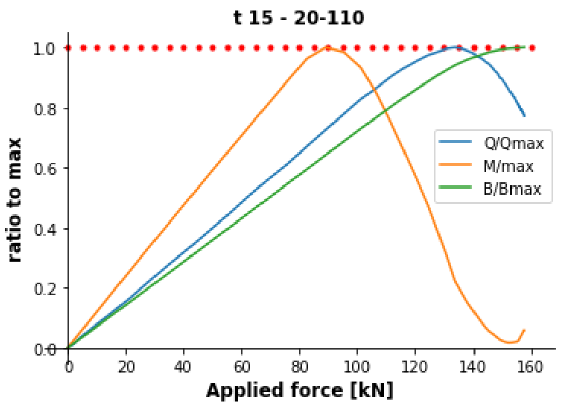

(c) t = 15 mm - n = 20 mm – w = 110 mm

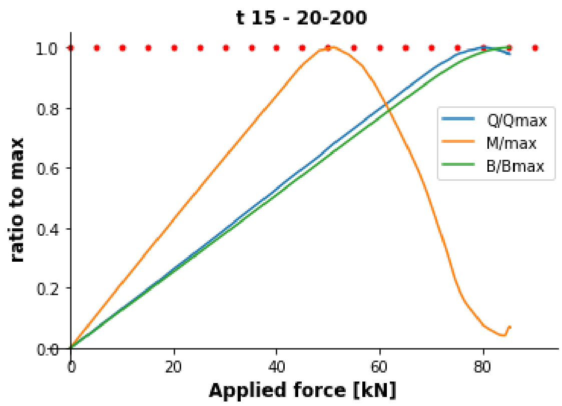

(d) t = 15 mm - n = 20 mm – w = 200 mm

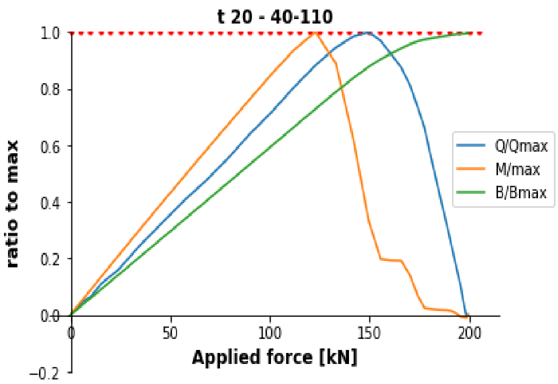

(e) t = 20 mm - n = 40 mm – w = 110 mm

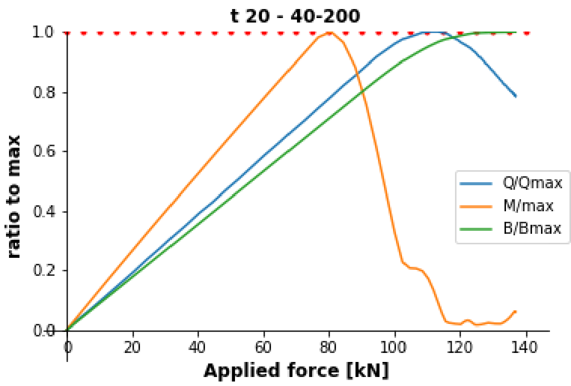

(f) t = 20 mm - n = 40 mm – w = 200 mm

Fig. 41. Ratio of Q, M and B to their Respective Maxima

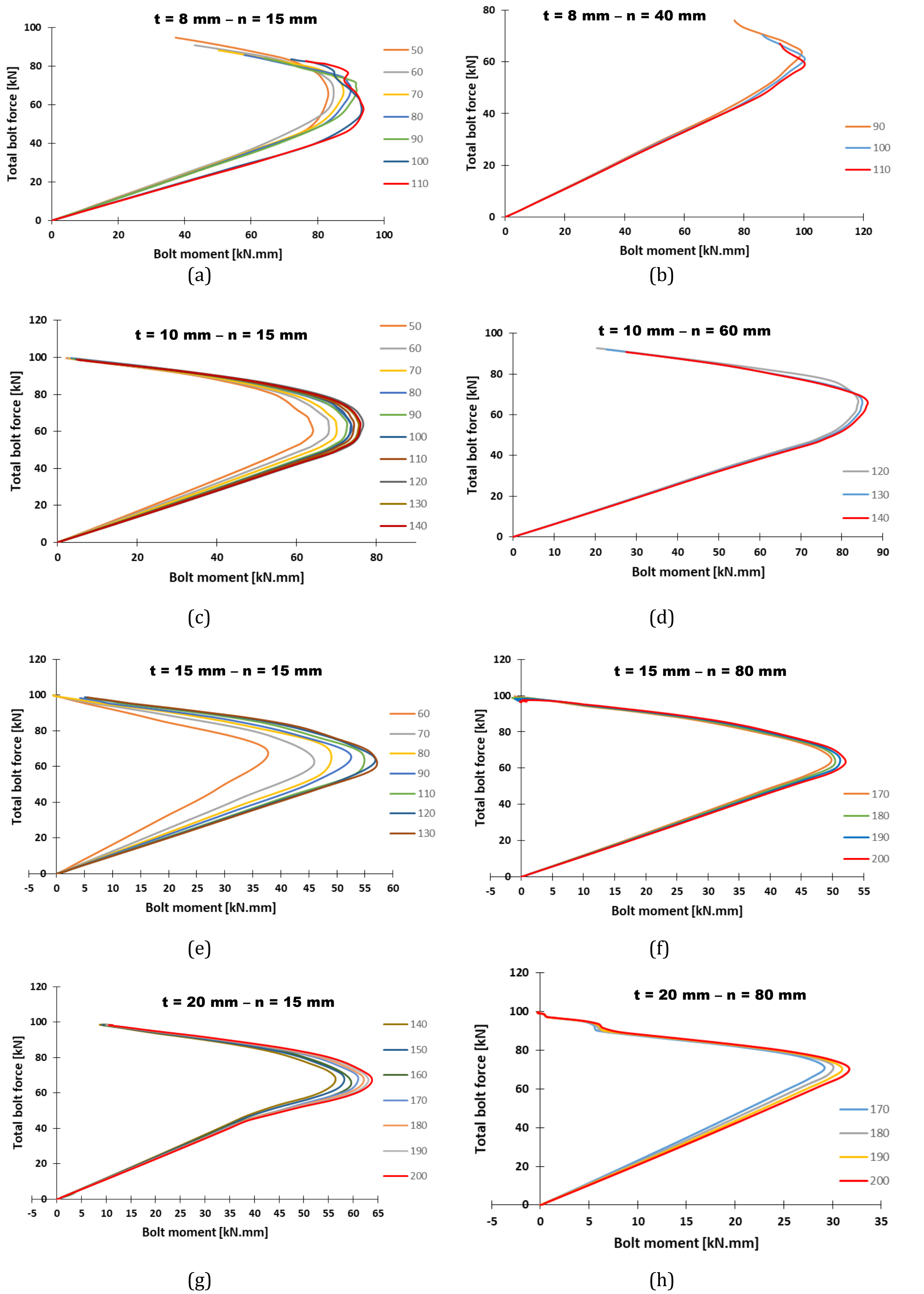

Fig. 42. Interaction Curves for t = 8 mm, 10 mm, 15 mm and 20 mm

4. Conclusion

The study carried out in this paper aimed to investigate prying effects in bolted T-stubs.

The focus was made on prying force Q, total bolt force B, bolt moment M, and their variations considering different values of flange thickness (t), edge distance (n) and gauge distance (w). The values of n and w were chosen to cover all the combinations allowed by EN 1993-1-8.

The main results of the work can be summarized as follows:

- The formulations presented in EN 1993-1-8 yield conservative estimations of the plastic resistance of T-stubs.
- In general, prying force and bolt moment exhibit the same variation pattern: an increase in gauge distance increases their values, and an increase in edge distance or thickness would decrease their values.
- Conversely, the total bolt force decreases as gauge distance increases and increases as edge distance or thickness increases.
- With non-preload bolts, the position of the resultant of the contact stresses is not dependent on the loading. Moreover, besides the flange and the bolt rigidities, the position depends heavily on the edge distance; whereas the gauge distance has negligible influence.
- The bolt moment can represent a substantial fraction (up to 65%) of the bolt flexural resistance, mainly in thin flanges where the deformation induces considerable bending of the bolts. Associated with the already significant tension of the bolts, it could cause a premature failure of the T-stub.
- A state of maximum prying force may not correspond to that of the maximum bolt force. Q_{max} and B_{max} are attained at almost the same load In thinner flanges. When thicker flanges are used, the point of maximum prying force and maximum bolt force are far apart for short gauge distances. However, as the gauge distance is increased, they tend to coincide.
- M_{max} is reached at earlier stages than Q_{max} and B_{max}. For all the specimens, B_{max} coincides with the total bolt force at ultimate load but this is not true for Q_{max} and M_{max}. Nevertheless, Q_{max} is equivalent to the prying force at ultimate load for specimens that exhibited a failure mode 1 or mode 2 close to 1. While the ultimate moment in the bolts was positive in all the specimens with thinner flanges, only a few specimens with thicker flanges exhibited a positive ultimate moment. Most specimens exhibited a negative moment at the ultimate stage, highlighting the predominance of the bolt tension over the bolt moment.

Considering the bending moment that may develop in the bolts is critical to a safer design of bolted steel connections. Considering that Q_{max} does not always correspond to B_{max}, it implies that, for design purposes, the maximum total bolt force should be considered. A better understanding of prying requires further investigations involving more key parameters such as steel grade, bolt diameter, bolt grade, the effective width of the T-stub, and considering a more comprehensive value range of flange thickness, edge distance, and gauge distance. The outcome may permit the development of an analytical model, including bolt bending and an accurate assessment of prying action (bolt moment and total bolt force).

Author Contributions

Author 1: Development of numerical models and execution of analyses; Author 2: Interpretation of results and writing the manuscript; Author 3: Alignment of models with theoretical background and conducting the literature review.

Declaration of Interests

The authors declare that they have no known competing financial interests or personal relationships that could have appeared to influence the work reported in this paper.

References

Abidelah A., Bouchaïr A., Kerdal D. E., Influence of the flexural rigidity of the bolt on the behavior of the T-stub steel connection, Engineering Structures 81 (2014) 181–194, http://dx.doi.org/10.1016/j.engstruct.2014.09.041

Aggerskov H. Analysis of bolted connections subjected to prying. Journal of the Structural Division ASCE; 103(ST11):2145-2163, 1977, https://doi.org/10.1061/JSDEAG.0004763

Atasoy M., Determinatıon of Prying Load on Bolted Connections. Ph.D. dissertation, Middle East Technical University, Ankara, Turkey (2012)

Bai R., Chan S.L., Hao J.P., Improved design of extended end-plate connection allowing for prying effects, J. Constr. Steel Res. 113 (2015) 13–27, https://doi.org/10.1016/j.jcsr.2015.05.008

Bai R., Chan S.L., Hao J.P., Improved design of extended end-plate connection allowing for prying effects, J. Constr. Steel Res. 113 (2015) 13–27, https://dx.doi.org/10.1016/j.jcsr.2015.05.008

Baoa W., Jianga J., Yua Z., Zhou X., Mechanical behavior of high-strength bolts in T-stubs based on moment distribution, Engineering Structures 196 (2019) 109334, https://doi.org/10.1016/j.engstruct.2019.109334

Bezerra L.M., Bonilla J., Silva W.A., Matias W.T., Experimental and numerical studies of bolted T-stub steel connection with different flange thicknesses connected to a rigid base, Engineering Structures 218 (2020) 110770, https://doi.org/10.1016/j.engstruct.2020.110770

Bursi O.S., Jaspart J.P., Basic issues in the finite element simulation of extended end plate connections, Computers and Structures 69 (1998) 361–382, https://doi.org/10.1016/S0045-7949(98)00136-9

Bursi O.S., Jaspart J.P., Benchmarks for finite element modelling of bolted steel connections, J. Constr. Steel Res. 43(1), 1997, pp17–42, https://doi.org/10.1016/S0143-974X(97)00031-X

Bursi O.S., Jaspart J.P., Calibration of a Finite Element Model for Isolated Bolted End-Plate Steel Connections, J. Construct. Steel Res. 44(3), 1997, pp. 225-262, https://doi.org/10.1016/S0143-974X(97)00056-4

Chasten C.P., Lu L.W., Driscoll G.C., Prying and shear in end-plate connection design, J Struct Eng 118 (5) (1992) 1295–1311, https://doi.org/10.1061/(ASCE)0733-9445(1992)118:5(1295)

Couchaux M., Hjiaj M., Ryan I., Bureau A., Effect of contact on the elastic behaviour of tensile bolted connections, J. Constr. Steel Res. 133 (2017) 459–474, https://doi.org/10.1016/j.jcsr.2016.10.012

DIN EN 14399-4:2006-06, High-strength structural bolting assemblies for preloading – Part 4: System HV – Hexagon bolt and nut assemblies

Douty R.T., McGuire W., High strength bolted connections with applications to plastic design, IABSE congress report, 1974, https://doi.org/10.5169/seals-7868

El Kalash S.N., Hantouche E.G., Prying effect in unstiffened extended end-plate connection with circular bolts configuration, J. Constr. Steel Res. 160 (2019) 402–410, https://doi.org/10.1016/j.jcsr.2019.05.043

El Kalash S.N., Hantouche E.G., Secondary prying of column flange in Tee-connections: Experimental investigation and mechanical modeling, J. Constr. Steel Res. 145 (2018) 518–528, https://doi.org/10.1016/j.jcsr.2018.03.012

EN 1993-1-8: Eurocode 3, design of steel structures – Part 1–8: Designs of Joints, 2005

Faralli A.C., Latour M., Tan P.J., Rizzano G., Wrobel P., Experimental investigation and modeling of T-stubs undergoing large displacements, J. Constr. Steel Res. 180 (2021) 106580, https://doi.org/10.1016/j.jcsr.2021.106580

Gantes C., Lemonis M., Influence of equivalent bolt length in finite element modeling of T-stub steel connections, Computers and Structures 81 (2003) 595–604, https://doi.org/10.1016/S0045-7949(03)00004-X

Girão Coelho A.M., Bijlaard F., Gresnigt N., Simões da Silva L., Experimental assessment of the behaviour of bolted Tstub connections made up of welded plates, J. Constr. Steel Res. 60 (2004) 269-311, https://doi.org/10.1016/j.jcsr.2003.08.008

Girão Coelho A.M., Bijlaard F., Simões da Silva L., Finite-Element Modeling of the Nonlinear Behavior of Bolted T-Stub Connections, J. Struct. Eng. 2006.132:918-928, https://doi.org/10.1061/(ASCE)0733-9445(2006)132:6(918)

Girão Coelho A.M., Characterization of the ductility of bolted end plate beam-to-column steel connections, Ph.D. dissertation, University of Coimbra, Coimbra, Portugal (2004)

Hantouche E.G., Abboud N.H., Stiffness modeling of bolted thick built-up T-stub connections including secondary prying effect, J. Constr. Steel Res. 95 (2014) 279–289, https://doi.org/10.1016/j.jcsr.2013.12.012

Hantouche E.G., Kukreti A.R., Rassati G.A, Swanson J.A., Modified stiffness model for thick flange in built-up T-stub connections, J.

Constr. Steel Res.81 (2013) 76–85, https://doi.org/10.1016/j.jcsr.2012.11.009

Hantouche E.G., Kukreti A.R., Rassati G.A., Investigation of secondary prying in thick built-up T-stub connections using non-linear finite element modeling, Engineering Structures 36 (2012) 113–122, https://doi.org/10.1016/j.jcsr.2013.12.012

Hantouche E.G., Kukreti A.R., Rassati G.A., Swanson J.A., Prying Models for Strength in Thick Flange Built-Up T-Stubs with Complete Joint Penetration and Fillet Welds, J. Struct. Eng. 141(2), 2015, https://doi.org/10.1016/j.jcsr.2012.11.009

Herrera R.A., Desjouis G., Gomez G., Sarrazin M., Behavior of welded t-stubs subjected to tensile loads, The 14th World Conference on Earthquake Engineering October 12-17, 2008, Beijing, China

Hu D., Papadopoulos J., Adams G.G., Prying action in an elastic T-stub tensile connection, J. Constr. Steel Res. 169 (2020) 106027

Kombate T.J.C., Taşkın K., State-of-the-art review on the behaviour of T-stubs and prying action, J. Constr. Steel Res. 191 (2022) 107203, https://doi.org/10.1016/j.jcsr.2022.107203

Kulak G. L., Fisher J. W., Struik J. H. A., Guide to Design Criteria For Bolted and Riveted Joints, 2nd Ed. New York: American Institute of Steel Construction (2001)

Mistakidis E. S., Baniotopoulos C. C., Bisbos C. D., Panagiotopoulos P. D., Steel T-Stub Connections Under Static Loading: an Effective 2-D Numerical Model, J. Construct. Steel Res. Vol. 44, Nos. 1-2, pp. 51-67, 1997, https://doi.org/10.1016/S0143-974X(97)00037-0

Nair R.S., Birkemoe P., Munse W., Behavior of Bolts in Tee-Connections Subject to Prying Action, Journal of the Structural Division, Vol. 353 (1969) pp. 161 – 175

Piluso V., Faella C., Rizzano G., Ultimate Behavior of Bolted T-Stubs. I: Theoretical Model J. Struct. Eng. 127 (2001), https://doi.org/10.1061/(ASCE)0733-9445(2001)127:6(686)

Piluso V., Faella C., Rizzano G., Ultimate Behavior of Bolted T-Stubs. II: Model Validation J. Struct. Eng. 127 (2001), https://doi.org/10.1061/(ASCE)0733-9445(2001)127:6(694)

Qiang X., Shen Y., Jiang X., Bijlaard F.S.K., Theoretical study on initial stiffness of thin-walled steel T-stubs taking account of prying force, Thin-Walled Structures 155 (2020) 106944, https://doi.org/10.1016/j.tws.2020.106944

Raebel CH, DeSimone R.G., Meier A.M., Effects of Bolt Spacing on Prying Forces in WT Connections, AEI 2013 - Building Solutions for Architectural Engineering, 2013, https://doi.org/10.1061/9780784412909.073

Sherbourne A.N., Bahaari M.R., 3D Simulation of Bolted Connections to Unstiffened Columns - I. T-stub Connections, J. Construct. Steel Res. Vol. 40, No. 3, pp. 169-187, 199, https://doi.org/10.1016/S0143-974X(96)00048-X

Simon M. W, Hengehold J. B., Finite Element Analysis of Prying Action in Bolted Joints, SAE Transactions, Vol. 86, Section 3: 770404–770718 (1977), pp. 2103-2112, https://doi.org/10.4271/770545

Stamatopoulos G.N., Ermopoulos J. Ch., Influence of the T-stub Flexibility on Its Strength, International Journal of Steel Structures, March 2010, Vol 10, No 1, 73-79, https://doi.org/10.1007/bf03249513

Steel Construction Manual, 16th Edition, AISC, USA, 2023

Swanson J.A., Kokan D., Leon, R., Advanced finite element modeling of bolted T-stub connection components. J. Constr. Steel Res. (2002) 58(5):1015–31, https://doi.org/10.1016/S0143-974X(01)00098-0

Swanson J.A., Leon R.T., Bolted steel connections: tests on T-stub components, Journal of Structural Engineering ASCE 2000;126(1):50–6, https://doi.org/10.1061/(ASCE)0733-9445(2000)126:1(50)

Tartaglia R., D'Aniello M., Zimbru M., Experimental and numerical study on the T-Stub behaviour with preloaded bolts under large deformations, Structures 27 (2020) 2137–2155, https://doi.org/10.1016/j.istruc.2020.08.039

Thornton W.A., Prying action - A general treatment, Eng J 22 (2) (1985) 67–75

Wanzek T., Gebbeken N., Numerical aspects for the simulation of end plate connections, In: Cost C1 WG6 report: Numerical simulation of semi-rigid connections by the finite element method, Virdi K.S (Ed.), European Commission, Brussels, 1999, pp 13-31

Yang J.G., Kim H.K., Park J.H., Back MC, Analytical Models for the Initial Axial Tensile Stiffness and Ultimate Tensile Load of a T-Stub, Including the Effects of Prying Action, International Journal of Steel Structures June 2013, Vol 13, No 2, 341-352, https://doi.org/10.1007/s13296-013-2012-7

Yang J.G., Park J.H., Kim H.K., Back MC, A Prying Action Force, and Contact Force Estimation Model for a T-Stub Connection with High Strength Bolts, Journal of Asian Architecture and Building Engineering, 2013, 12:2, 309-316, https://doi.org/10.3130/jaabe.12.309

Yuan H.X., Hu S., Du X.X, Yang L., Cheng X.Y., Theofanous M., Corrigendum to "Experimental behaviour of stainless steel bolted T-stub connections under monotonic loading" [J. Constr. Steel Res. 152(2019) 213–224], J. Constr. Steel Res. 172 (2020), https://doi.org/10.1016/j.jcsr.2019.105860

Yuan H.X., Hu S., Du X.X, Yang L., Cheng X.Y., Theofanous M., Experimental behaviour of stainless steel bolted T-stub connections under monotonic loading, J. Constr. Steel Res. 152 (2019) 213–224, https://doi.org/10.1016/j.jcsr.2018.02.021

Zhao M.S., Lee C.K., Fung T.C., Chiew SP, Impact of welding on the strength of high-performance steel T-stub joints, J. Constr. Steel Res. 131 (2017) 110–121, https://doi.org/10.1016/j.jcsr.2016.12.023

Zoetemeijer P., A design method for the tension side of the statically loaded, bolted beam to column connections, *Heron,* 1974, 20(1), 59